

# The interface reactions between ash from biofuels and limestone



Limestone quarry in Brønnøy, Norway [26]

Leane van Dijk

Umeå University Department of  
Applied Physics and Electronics  
Fontys University of Applied Science

Bachelor thesis 2020/2021

# The interface reactions between ash from biofuels and limestone

The effect of ash from the biomasses wheat straw, forest residues and DDGS at the product quality of quicklime

Bachelor thesis

Author:

Leane van Dijk

Applied Science

3363155

[Leane.vandijk@student.fontys.nl](mailto:Leane.vandijk@student.fontys.nl)

Study:

Applied Science

Fontys University of Applied Science

Eindhoven

Supervisor:

Yvonne van Lith

Internship:

Umeå University

Department of Physics and Electronics

Prof. Markus Broström



1 November 2020 – 15 June 2021

Sweden

## Summary

Limestone is a sedimentary rock that is composed mostly of calcium carbonate ( $\text{CaCO}_3$ ). Limestone is, among many applications, used as a raw material for the manufacture of quicklime. When limestone is heated, the stone calcinates and quicklime is formed. The primary use of quicklime is in the steel and building industries.

For quicklime production, process temperatures above  $1000^\circ\text{C}$  are required. Nowadays, to achieve this process temperature, fossil fuels such as coal, natural gas and oil are the main sources of energy. The disadvantage of using fossil fuels is the amount of  $\text{CO}_2$  that is released into the atmosphere. Beside the  $\text{CO}_2$  emissions due to burning fossil fuels,  $\text{CO}_2$  is also a product of limestone decomposition, which is released during the heating process. To reduce  $\text{CO}_2$  emissions, converting the process from using fossil fuels to biofuels is a promising possibility.

In existing kilns for quicklime production, fuel and combustion air are in direct contact with the stone. That means ash-forming elements in the fuel could possibly affect both the process and the product quality. The purpose of this study is to analyse how different ashes from the biomasses wheat straw, logging residues and DDGS (Distillers Dried Grain with Solubles) affect the product quality of the quicklime. Each biomass tested has a different ash composition, representing groups of biofuels with high potassium and silicon content, high calcium content, and high phosphorus content, respectively. These three biomasses are all from residual streams, which means that they don't contribute to deforestation and food competition.

In this study, a tube furnace was used to simulate the conditions in an industrial rotary kiln. In the tube furnace, limestone was exposed to the ash from the biomasses for 25 minutes at two different temperatures,  $1100^\circ\text{C}$  and  $1350^\circ\text{C}$ . After the exposure, the quicklime samples were analysed with a SEM (Scanning Electron Microscope) with an EDS (Energy Dispersive Spectrometer). The ash infiltration, changes in microstructure and reactions from ash-forming elements in the exposed material were analysed. Besides the elemental analyses, changes in the microstructures were analysed with help of the programmes ImageJ and Matlab.

In all the samples, the ash of the biomass infiltrated in the quicklime. The wheat straw samples had the most infiltration, followed by the DDGS. The forest residue samples had the least ash infiltration. In both the wheat straw and forest residues, K, Ca and Si is found, possibly in the form of a K-Ca-silicate. The DDGS samples proved that the calcium and phosphorus are attracted to each other. Beside phosphorus, potassium had also infiltrated.

To analyse the microstructure in Matlab, binary images were provided with ImageJ. For all binary pictures, the functions 'Smooth' and 'Auto Local Threshold; Otsu; Radius 20' were used. The microstructure analyses verified that ash from the biomass affects the microstructure of the quicklime at the interface. In comparison with the reference samples, the quicklime samples exposed to biomass ash had a higher porosity at the interface. Between the samples exposed to the biomass ash, there is no visible difference between the  $1100^\circ\text{C}$  and the  $1350^\circ\text{C}$  quicklime samples. This is in contrast to the reference samples, whose structures differs significantly between the samples exposed at  $1100^\circ\text{C}$  and  $1350^\circ\text{C}$ .

A proposal which biomass should be the best option to substitute coal as fuel in the heating process of the quicklime manufacturing, can't be made. For that more analyses are needed. Nevertheless, it can be concluded that all tested biomasses affect the microstructure at the interface of the quicklime samples, and the ash of the biomasses infiltrates at the interface of the quicklime and interactions between elements occurs.

## Acknowledgements

I am thankful for the opportunity I had to do my bachelor thesis abroad. For that I would like to thank the centre for Sustainable Cement and Quicklime Production at Umeå University and the manager Matias Eriksson. I thank Markus Broström for his trust, Karin Sandström for all her support and Yvonne van Lith for supervising me. I also want to thank Markus Calborg for his assistance throughout the project and Cheng Choo Lee for her assistance while using the Scanning Electron Microscope. Finally I would like to thank all my colleagues too for their sociability that allowed me I feel at home.

## Table of contents

Summary .....	II
Acknowledgements .....	III
Table of contents .....	IV
1. Introduction.....	1
2. Theoretical background.....	2
2.1 Limestone .....	2
2.1.1 Limestone manufacturing .....	3
2.2 Quicklime.....	4
2.2.1 Calcination .....	4
2.3 Fuel .....	5
2.3.1 Wheat straw .....	5
2.3.2 Forest residues .....	5
2.3.3 DDGS.....	5
2.4 Combustion of biomass.....	6
2.5 Rotary kiln.....	7
2.6 SEM with EDS.....	8
3. Research strategy .....	10
3.1 Hypothesis .....	10
3.1.1 Wheat straw .....	10
3.1.2 Forest residues .....	11
3.1.3 DDGS.....	11
4. Experimental .....	13
4.1 Ash preparation.....	13
4.2 Limestone preparation.....	13
4.3 Limestone exposure .....	13
4.4 Sample preparation for SEM analyses.....	14
4.5 Sample analysis .....	14
4.5.1 Structure analysis .....	14
4.6 Risk analysis.....	15
4.6.1 Hot surfaces.....	15
4.6.2 Reactivity quicklime.....	15
5. Results .....	16
5.1 Ash composition after combustion .....	16
5.2 Samples overview.....	17
5.3 Reference .....	18

5.4	Ash composition after exposure .....	18
5.5	Ash infiltration.....	21
5.6	Structure.....	26
5.6.1	Threshold.....	26
5.6.2	Pore analysis.....	27
6.	Discussion.....	29
6.1	Results from experimental work.....	29
6.1.1	Wheat straw .....	29
6.1.2	Forest residues .....	29
6.1.3	DDGS.....	30
6.2	Structure analysis .....	30
7.	Conclusion .....	32
8.	Recommendations.....	33
9.	Reference list.....	34
	Appendix A .....	36
	Appendix B .....	37
	Appendix C.....	40
	Appendix D .....	43
	Appendix E.....	47

## 1. Introduction

Limestone is a sedimentary rock that is found naturally in the earth's environment [1][2]. It is composed mostly of calcium carbonate ( $\text{CaCO}_3$ ). Today, the usage of limestone covers a wide range of applications. It is used in the construction industry, the iron and steel industry, the chemical industry and it is the raw material for the manufacture of quicklime, slaked lime, cement and mortar.

There is a great need for strengthening the research in production of limestone-based products, especially in the high temperature processes where substantial amounts of carbon dioxide are generated. Quicklime is one of those limestone-based products [3]. When limestone is heated, the stone calcinates and quicklime is formed. The primary use of quicklime is in the steel industry as flux or in the building industry in the manufacture of calcium silicate bricks, mortar, plaster and limewash.

Fossil fuels such as coal, natural gas and oil are today the main sources of energy to achieve the process temperatures above  $1000^\circ\text{C}$  needed for quicklime production [3]. The disadvantage of using fossil fuels is the amount of  $\text{CO}_2$  that is released in the atmosphere. Besides  $\text{CO}_2$  emissions due to burning the fossil fuels,  $\text{CO}_2$  is also a product of limestone decomposition, which is released during the heating process.

Nowadays, in light of climate change, it is important to reduce  $\text{CO}_2$  emissions. Biofuels are considered carbon neutral. Biomass absorbs atmospheric  $\text{CO}_2$ . During the combustion process of biomass,  $\text{CO}_2$  is released into the atmosphere and, due to the relatively short cycle, this process can be considered  $\text{CO}_2$  neutral. Therefore, converting the process of quicklime production from using fossil fuels to biofuels is a promising way to reduce the amount of  $\text{CO}_2$  emitted.

The use of biofuels in quicklime production has not yet been evaluated. In existing kilns, fuel and combustion air are in direct contact with the stones. That means ash-forming elements in the fuel could possibly affect both the process and the product quality. The purpose of this study is to analyse how different ashes from the biomasses wheat straw, forest residues and DDGS (Distillers Dried Grain with Solubles) affect the product quality of quicklime. Each biomass tested has a different ash composition, representing groups of biofuels with high potassium and silicon content, high calcium content, and high phosphorus content, respectively.

The effect of the ash will be tested by using a tube furnace purged with  $\text{CO}_2$  and  $\text{O}_2$  gases. In the furnace, the limestone will be exposed to the ash from the biomasses at two different temperatures,  $1100^\circ\text{C}$  and  $1350^\circ\text{C}$ . After the exposure of the limestone in the furnace, the samples will be analysed with the SEM (Scanning Electron Microscope) with an EDS (Energy Dispersive Spectrometer). The ash infiltration, changes in microstructure and distribution of ash-forming elements in the exposed material can be analysed with the SEM/EDS. Subsequently, the microstructure of the quicklime can be analysed and compared with help of the programmes ImageJ and Matlab.

First, the theoretical background with information about the limestone, quicklime, the calcination process, the biomasses and the equipment used will be discussed. Subsequently, the research strategy with the hypothesis will be explained and the experimental will be specified, whereupon the results will be presented. The results will be discussed accordingly and a conclusion will be formulated. Finally, a recommendation is made for possible additional research.

## 2. Theoretical background

This study includes two important parts, the calcination process of the limestone and the specifications of the biomass ash. In this section, first the limestone and its manufacturing will be explained to create an understanding of the origin of limestone. Afterwards, the calcination process and the uses of quicklime will be discussed. The fuel used in the production process of calcination will be discussed in general. Whereupon, the specific biomasses used and the combustion of biomass will be described. Finally, the working principle of the tube furnace and the SEM/EDS will be revealed. All of this theory is necessary to make a good hypothesis concerning the research outcome.

### 2.1 Limestone

Limestone is a carbonate sedimentary rock principally composed of calcium carbonate ( $\text{CaCO}_3$ ) in the form of calcite or occasionally aragonite [1][2][4]. Typically, high purity limestones contain more than 98%  $\text{CaCO}_3$ . The remaining part may consist of small amounts of silicon, magnesium, aluminium, iron, sodium and titanium. The minerals aragonite and calcite are different crystal forms of calcium carbonate. Aragonite is metastable under ambient conditions and converts to calcite. Dolomite is a similar sedimentary rock in which calcium magnesium carbonate ( $\text{CaMg}(\text{CO}_3)_2$ ) predominates. Around 20% of all sedimentary rocks are limestone or dolomite. Common impurities in sedimentary carbonate rocks include clay minerals, silica, organic matter and iron oxyhydroxide minerals. In this study, the focus is on pure limestone.

Most limestones form in shallow, calm, warm marine waters where organisms are capable of generating calcium carbonate shells and skeletons [5]. When these organisms die, their shell and skeletal debris accumulate as a sediment that might be lithified into limestone. Limestones formed from this type of sediment are biological sedimentary rocks. The biological origin can be recognised by the presence of fossils. Other limestones are formed by direct precipitation of calcium carbonate from marine or fresh water. Limestones formed this way are chemical sedimentary rocks.

Limestone is a rock with an enormous diversity of uses [4]. The primary use of limestone is in construction as aggregate or in the production of cement. It is also extensively used in the iron and steel industry, in the chemicals industry and in the manufacture of glass. In these non-constructural applications, limestone may be used either as a chemically reactive raw material or as an inert filler or pigment. Figure 1 shows an overview of the uses of limestone.

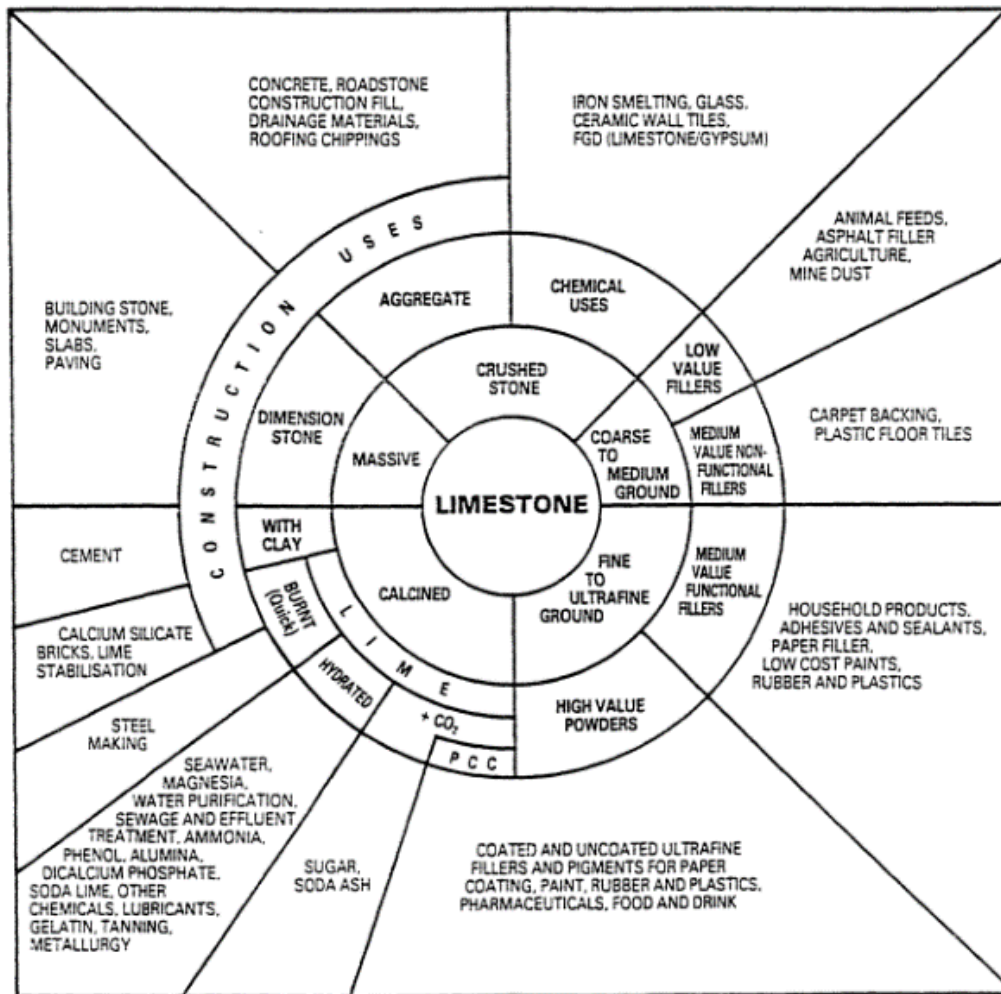


Figure 1 Processing and major uses of limestone [4]

### 2.1.1 Limestone manufacturing

The raw material, such as high purity limestone, is quarried, pre-crushed and washed and then screened before being transported to the lime plant [6]. Limestone is normally obtained by surface quarrying, generally adjacent to the lime plant so that the raw material can be transported directly to the plant. Subsequently, the limestone is charged into a kiln where it undergoes a thermal decomposition reaction and becomes quicklime. The quicklime is generally crushed, milled and/or screened before the product is transported to the end user for use in the form of quicklime, or transferred to a hydrating plant where it will react with water to produce hydrated or slaked lime. Figure 2 shows the steps involved in the overall limestone manufacturing process.

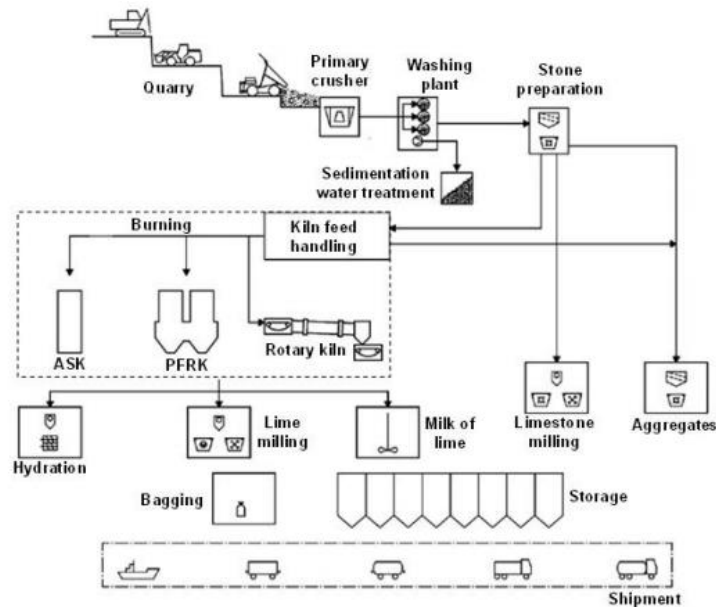


Figure 2 Overview of the limestone manufacturing process [6]

## 2.2 Quicklime

Calcium oxide (CaO), commonly known as quicklime or burnt lime, is a widely used chemical compound [3]. The primary use of quicklime is in the steel industry as flux to remove silica, sulphur and phosphorus from pig iron, or in the construction industry in the manufacture of calcium silicate bricks, mortar, plaster and limewash (Figure 1). Quicklime is made by thermal decomposition, or calcination, of limestone. Quicklime contains mostly CaO, while the remaining fraction consists of small amounts of silicon, magnesium, aluminium, iron, sodium and titanium.

### 2.2.1 Calcination

In quicklime production, limestone is heated in an industrial kiln. During heating, carbon is released from the limestone as carbon dioxide gas. Quicklime remains as a solid product. The calcination can be described by reaction 1.



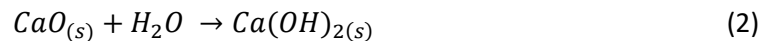
Calcination is an endothermic reaction with a theoretical energy use of 177.8 kJ/mol<sub>CaO</sub>, that is 3.2 GJ/ton<sub>CaO</sub>.

The decomposition of limestone starts with the transfer of heat to the particle surface and through the CaO and CaCO<sub>3</sub> layers to the reaction zone [3]. Subsequently, a chemical reaction occurs and afterwards, the CO<sub>2</sub> gas migrates through the CaO layer and will be released to the atmosphere. The released CO<sub>2</sub> is equal to a total weight loss of 44% [7].

Numerous factors influence the calcination process, e.g. particle size, porosity, the defect density and purity of limestone, burning temperatures, retention time in the kiln and pCO<sub>2</sub> [8]. pCO<sub>2</sub> is the partial pressure of CO<sub>2</sub>.

Under air circumstances, the thermal decomposition of calcite takes place at around 700°C [3][9]. The partial pressure of CO<sub>2</sub> influences the type of decomposition reaction and the onset temperature. An increasing pCO<sub>2</sub> influences the full decomposition equilibrium so that a higher temperature is needed for decomposition. During calcination, pCO<sub>2</sub> will increase due to the formed CO<sub>2</sub>, a higher temperature is required for further decomposition. However, in this study, this is negligible because of the small sample size.

Quicklime is a reactive solid. When quicklime contacts water, the quicklime releases thermal energy via the formation of calcium hydroxide [8]. This hydration reaction of quicklime is an exothermic reaction and can be expressed by reaction 2:



This is an exothermic reaction with a theoretical energy release of 64.5 kJ/mol<sub>CaO</sub>.

### 2.3 Fuel

The lime industry is a highly energy intensive industry, with energy accounting for up to 60% of total production costs. In the process, the fuel provides the necessary energy for calcining [6][3]. The most commonly used fuels in the EU are fossil fuels such as natural gas, coke oven gas, coal, coke and fuel oil. The combustion of fossil fuels provides energy in the form of heat. Beside heat, CO<sub>2</sub> is a product that is released into the atmosphere. For quicklime production, an estimated 20-32% of the CO<sub>2</sub> emissions are combustion emissions. The other 68-80% are process emissions (the CO<sub>2</sub> which releases during the calcination reaction (reaction 1)) [3]. Of all the greenhouse gas emissions that have been identified to contribute to climate change, CO<sub>2</sub> is described as the dominate one. It is important to reduce CO<sub>2</sub> emissions; recently awareness has increased even more. Biofuels can be considered more carbon neutral than fossil fuels. One promising way to reduce the amount of CO<sub>2</sub> released is to convert the industries from using fossil fuels to biofuels. Biomass is regarded as a fuel with high potential due to the fact that it could be integrated into existing kilns without major rebuilding.

Hence, the fuel interacts with the process and the combustion products. The ash of the burned biomass comes into contact with the quicklime. In this study, the effect of the ash from the three biomass fuels wheat straw, forest residues and DDGS on the limestone will be tested. These three biomasses are all from residual streams, meaning that they don't contribute to deforestation and food competition other than land use. In the subsequent subsections, the three biomasses will be discussed.

#### 2.3.1 Wheat straw

Straw is an agricultural by-product consisting of the dry stalks of cereal plants after the grain and chaff have been removed [10][11]. Wheat straw is the straw especially from wheat. Traditionally, straw is treated as waste. However, the straw still has value and can be used in various ways, such as fuel, livestock bedding and fodder, thatching and basket making. Straw is a residue from food production and this makes it useful as biomass fuel.

#### 2.3.2 Forest residues

Forest residues are a by-product from forest harvesting [12]. This includes thinning, cutting stands for timber or pulp, clearing lands for construction, or other uses that also yield tops and branches usable for bioenergy. Forest residues have been, just like wheat straw, underutilised and treated as waste materials for a long time, because of their high collection and transportation costs, as well as their low market value [13]. While open burning is often employed to dispose of forest residues, this practice generally results in substantial negative economic and environmental impacts.

#### 2.3.3 DDGS

Distillers dried grain with solubles (DDGS) is a cereal by-product of wheat-based ethanol production [14]. Wheat grain is the most common feedstock for ethanol in the EU. However, only around 50% of the energy in wheat grain can be converted into ethanol. About 30 wt% (weight percent i.e., the mass fraction of a substance within a mixture) of the grain feed stock is converted to wheat DDGS. This DDGS is mainly used as a source of protein and energy for livestock.

## 2.4 Combustion of biomass

Biomass absorbs atmospheric CO<sub>2</sub> as well as nutrients from the ground [15]. During the combustion process, the CO<sub>2</sub> is released into the atmosphere and due to the relatively short cycle this process can be considered CO<sub>2</sub> neutral. However, using biomass is not totally CO<sub>2</sub> neutral. For the conversion of the biomass to a manageable condition for use as a fuel, there is a regularly process needed that still results in emissions of CO<sub>2</sub>. The chemical composition and the combustion properties of biomass vary greatly depending on the agricultural species from which the biomass originates and the seasonal and regional variance of the feedstock.

Combustion is defined as the exothermal reaction between fuel and oxygen to form mainly CO<sub>2</sub> and water vapour. The heat released can be used in several ways. The basic combustion route of a solid fuel is the following: when the biomass is heated, first the water will evaporate. Subsequently, volatiles are released from the fuel as a gas when heated and they combust when mixed with oxygen. The remaining charcoal will predominantly retain its original shape and will be oxidised until the solid residue is ash.

The ash content and composition vary considerably between feedstocks, ranging from below 0.5 wt% db in wood pellets produced from debarked stem wood to 5-10 wt% db in agricultural residues, straw and miscanthus. The dry basis (db) is a measure of how much water is in a solid, which is expressed as the weight of water as a percentage of the completely dry solid. In case of the ash content in wt% db, the water content is evaporated before the ash content is determined. The concentrations of the major ash-forming elements in biomass, such as Si, K, Na, S, Cl, P, Ca, Mg and Fe, are of great importance for combustion characteristics [16].

The ash compositions of the used biomasses wheat straw, forest residues and DDGS are shown in Figure 3.

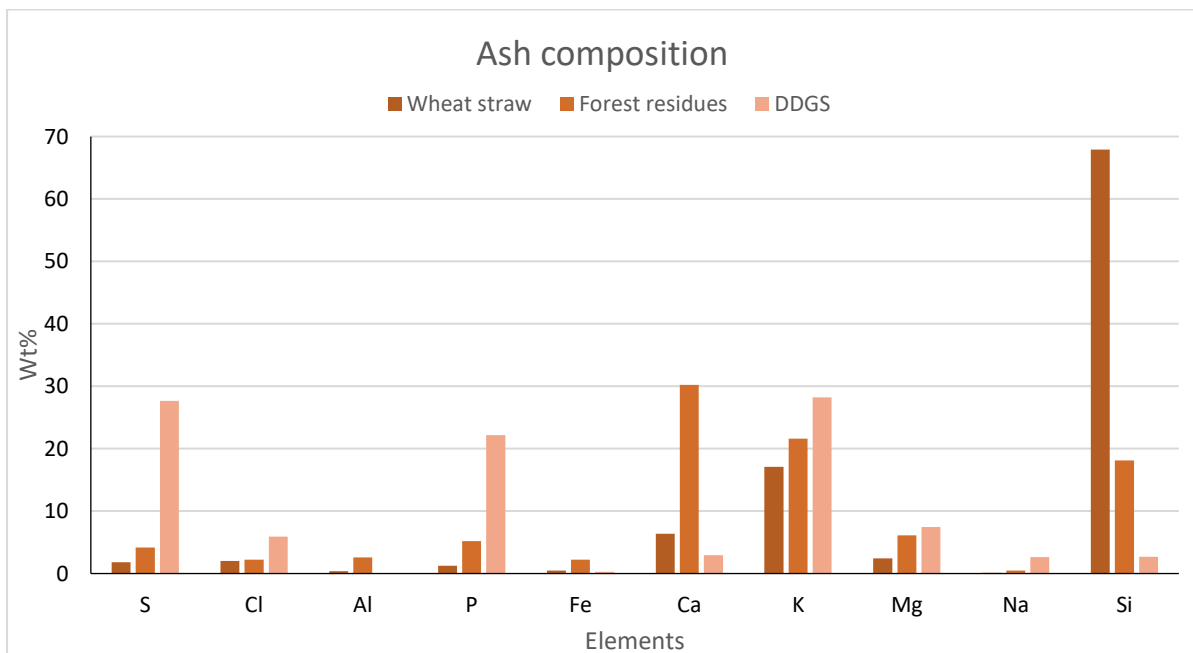


Figure 3 Ash composition of the biomasses

## 2.5 Rotary kiln

One way for quicklime production is to use a rotary kiln. A rotary kiln is a large steel tube that is lined on the inside with refractory bricks [17]. In the kiln, the limestone is heated and quicklime will be created. They are slightly inclined from the horizontal and are slowly rotated on a set of riding rings. Limestone is introduced at the uphill and the feed makes its way slowly to the discharge end due to the inclination and rotation. A burner is installed at the downhill or discharge end of the kiln where fuel is burned to form a cylindrical flame. This flame and the hot combustion gases that flow up the kiln dry, heat and calcine the counter-flowing lime solids. Figure 4 and Figure 5 show a schematic of the exterior and interior features of a rotary kiln.

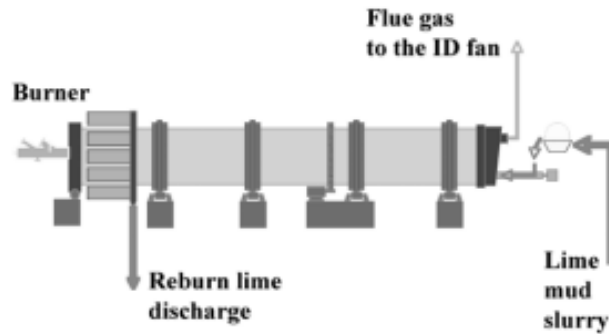


Figure 4 Exterior of a rotary kiln [17]

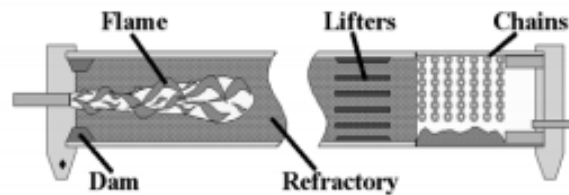


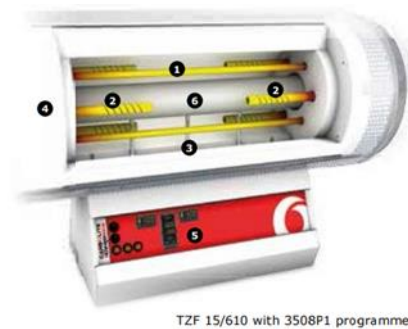
Figure 5 Interior of a rotary kiln [17]

In this study, the tube furnace Carbolite Gero STF 16/450 (Figure 6) was used. The tube furnace was used to simulate the conditions of an industrial rotary kiln. The maximum kiln temperature is 1600°C. Figure 7 shows the interior of a tube furnace at laboratory scale. This is a different type than the one used during this study, therefore point 5 mentioned in figure 7 is irrelevant.

In the tube furnace, it is possible to create a CO<sub>2</sub> rich environment. The furnace heats up at a rate of 3°C/min. This low heating rate is set mainly because of the ceramic tube. If the heating rate is too high, the tube can be affected. When the tube received the set point temperature, the sample can be placed in the middle of the tube furnace to achieve a high sample heating rate. Here is the centre zone of the heating element.



Figure 6 Tube furnace used for the experiments



- |                                |                       |
|--------------------------------|-----------------------|
| 1) Centre zone heating element | 4) Thermal insulation |
| 2) End zone heating elements   | 5) Work tube          |
| 3) Control thermocouples       | 6) Work tube          |

Figure 7 Schematic of a tube furnace at lab scale [18]

## 2.6 SEM with EDS

A SEM (Scanning Electron Microscope) is a type of electron microscope that produces images of a sample by scanning the surface with a focused beam of electrons [19][20]. Electrons have much shorter wavelengths than light, enabling better resolutions.

Figure 8 shows a schematic of the SEM. In this research the Carl Zeiss Evo was used. The electron gun emits and accelerates electrons towards the optics column. The main part of the machine is contained within a sealed vacuum chamber, because electrons will not travel freely through air. Besides that, the vacuum prevents electrons from being scattered by gas molecules and electron-induced chemical reactions. The condenser lens converges and demagnifies electrons into small beam size. Then, the scan coil rasters the electron beam across the sample surface and the objective lens controls the final focus of the beam onto the sample surface. Afterwards, the electron beam hits the sample. The interaction of electrons within a sample will generate backscattered and secondary electrons. These signals are collected by the detectors and generate an image and elemental information.

EDS (Energy Dispersive Spectroscopy) is a chemical microanalysis technique used in combination with SEM [21]. In this research, the Oxford instruments X-Max 80 mm<sup>2</sup> was used. The EDS technique detects X-rays emitted from the sample when the electron beam hits the sample. The spectrum of X-ray energy versus counts is evaluated to determine the elemental composition of the sampled volume. The characterisation capabilities are due in large part to the fundamental principle that each element has an unique atomic structure allowing unique sets of peaks on its X-ray spectrum. The

positions of the peaks in the spectrum identify the element, whereas the intensity of the signal corresponds to the concentration of the element.

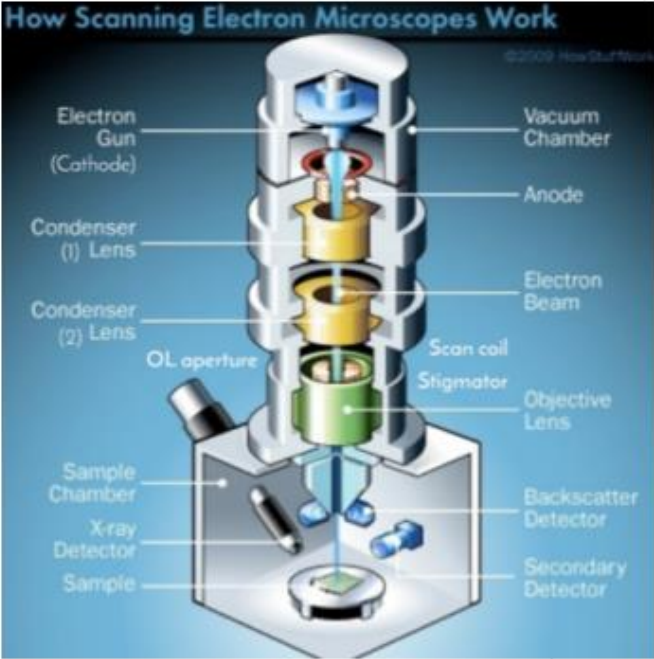


Figure 8 Schematic of a SEM [22]

### 3. Research strategy

The theoretical background supports the understanding of the calcination process and the composition of the ashes from the biomasses. With this theory, it is possible to propose a research strategy.

In this study, the limestone will be heated under a high CO<sub>2</sub> atmosphere. The reason for this is to imitate the industrial process. In the industry, CO<sub>2</sub> is released by the combustion of the fuel and as a by-product during the calcination. Since in this study the biomass is already burned and only the ash will be added to the limestone sample, there is a smaller amount of CO<sub>2</sub>, only as result of the calcination.

In the experiments, the burning time will be 25 minutes. An experiment had shown that a limestone sample with the same dimensions and circumstances is fully calcinated after 15 minutes. However, to be sure that all the possible reactions between the ash and the quicklime are accomplished, the stone will be heated an additional 10 minutes.

The industrial heating process occurs mainly in rotary kilns at temperatures of 900-1200°C. These temperatures are sufficiently high in order to liberate CO<sub>2</sub> and to obtain the desired oxide. In this study, a tube furnace at laboratory scale will be used with temperatures of 1100°C and 1350°C. At both temperatures, the limestone will calcinate. These are relevant temperatures for the industry, 1350°C corresponds to the limestone close to the flame and 1100°C to the limestone located further from the flame (Figure 5).

Beside the several samples with biomasses, a reference will be exposed at both 1100°C and 1350°C. The reference sample has the same dimensions, but it doesn't contain ash. This is important to estimate if the possible change in microstructure is a consequence of the calcination, the high temperature, the high CO<sub>2</sub> atmosphere, or of the ash.

The three biomasses that will be tested are: wheat straw, forest residues and DDGS (Distillers Dried Grain with Solubles). Each biomass has a different ash composition representing groups of biofuels with high potassium and silicon content, high calcium content, and high phosphorus content, respectively.

To figure out if any reaction occurred during the exposure of the limestone to the ash, the samples will be analysed with the SEM/EDS. The electrons, which the SEM uses, have much shorter wavelengths than light. This enables better resolutions than a light microscope. With the EDS, the elemental composition of the sampled volume can be determined. With this information, the possible reactions between the ash of the biomass and the CaO in the limestone can be analysed.

#### 3.1 Hypothesis

The expectation is that all limestone samples will calcinate and will convert to CaO. However, in the quicklime samples exposed with the biomass ash, it is possible that the ash will infiltrate into the stone. This could lead to chemical reactions in the stone and a possibly microstructural change. In the subsequent subsections, this will be explained per biomass.

The ash of the biomasses at 1350°C are probably more melted than the ash at 1100°C, therefore the expectation is that there is more ash infiltration at 1350°C.

##### 3.1.1 Wheat straw

Wheat straw has an ash content of 9.7%. That means that after the combustion, 9.7 wt% of the pellets remain in ash form. Wheat straw contains a high concentration of potassium and silicon and a

low concentration of calcium (Figure 3). With help of the ternary phase diagram of the SiO<sub>2</sub>-K<sub>2</sub>O-CaO system and the concentrations of the elements, it is found that the melting temperature of the ash will be around 800°C (Appendix A, Figure A1).

The expectation is that potassium will partially vaporise as K (g) and that the remaining K will interact in the oxide form with SiO<sub>2</sub> according the following reaction [16][23]:



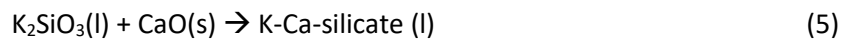
This product is stable and molten in residual ash.

Silicon is more affected to K than to CaO, which is formed in the stone during the calcination process. However, there is a possibility that the SiO<sub>2</sub> will interact with the CaO according to:



This is a slow reaction with a stable and solid product.

It's more likely that the K<sub>2</sub>SiO<sub>3</sub> in the molten ash will interact with the CaO in the limestone according to the following reaction:



The question is how far the K<sub>2</sub>SiO<sub>3</sub> will enter the stone before it will interact with the CaO.

### 3.1.2 Forest residues

Forest residues have an ash content of 1.8% and have, just like wheat straw, a high concentration of K and Si [16]. Besides that, forest residues also have a high Ca concentration. Due to the higher Ca concentration, the melting temperature is higher than the melting temperature of wheat straw (Appendix A, Figure A1).

The ash contains K, Si and Ca. The expectation is that, just as wheat straw, K<sub>2</sub>SiO<sub>3</sub>(l) (reaction 3) will be formed. The ash contains Ca, therefore the expectation is that the K<sub>2</sub>SiO<sub>3</sub> will directly interact with the CaO in the ash, instead of the CaO in the limestone, according to reaction 5. The K-Ca-silicate is a liquid, whereby this could enter the stone.

### 3.1.3 DDGS

DDGS has an ash content of 4.4%. DDGS has a high concentration of K, P and S and is the most difficult one to predict since the Ca-P-K system is only partly known.

The expectation is that S will vaporise as SO<sub>3</sub> (g) or SO<sub>2</sub> (g) [16][24]. This could already happen during the combustion of the DDGS pellets. If the S will not volatilise, SO<sub>3</sub> could interact with CaO in the limestone according to reaction 6.



This product is a solid in the ash and stable till 1200°C.

Another expectation is that P and K in the ash will interact according to the following reaction:



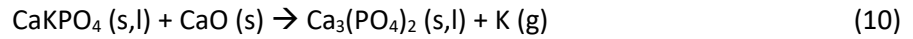
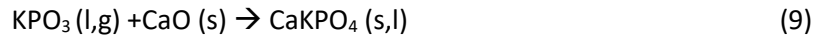
The product is molten and will be partially volatile in residual ash.

K is more affected to P than to CaO (which is the main part of the limestone). However, there is a possibility that the P<sub>2</sub>O<sub>5</sub> will interact with the CaO in the limestone according to:



This is a stable and solid product.

It's more likely that the KPO<sub>3</sub> in the molten ash will interact with the CaO in the limestone according to the following reactions:



Reaction 9 and 10 can happen because of the abundant available CaO in the limestone. K will volatilize during this reaction.

## 4. Experimental

The interaction between ash and limestone during calcination is tested in a furnace. To inspect the interaction between ash, coming from the fuel, and the limestone during the calcination, a tube furnace is used. Limestone samples with ash were heated for 25 minutes in the tube furnace. The three different ashes from the biomasses wheat straw, forest residues and DDGS and a reference were tested at both 1100°C and 1350°C.

### 4.1 Ash preparation

The biomass that was used was in the form of pellets. To obtain ash, the biomass was combusted in a furnace. The biomass was first heated for 60 minutes at 250°C, afterwards the biomass was heated at 550°C overnight. However, all three biomasses weren't fully burned, because the ash still contained black pieces. Black pieces represent the presence of carbon. Therefore, the ash was crushed and placed again in a kiln at 550°C overnight. To be sure that all the carbon has left, the ash was weighed and heated again at 550°C for one hour. After that hour, the ash was weighed again. The weight was identical. Due to this, it was assumed that all the carbon had left and the biomass was fully burned. The last step was crushing the samples. After crushing, the ash was a fine powder.

### 4.2 Limestone preparation

The sample preparation consists of several steps. 11 samples were prepared, 2 samples for each biomass, 2 reference samples and 3 additional samples in case something unexpected would happen with one of the other samples. The used limestone batch is high purity limestone and has the following composition: 98 wt% CaO, 0.9 wt% SiO<sub>2</sub>, 0.1 wt% Al<sub>2</sub>O<sub>3</sub>, 0.1 Fe<sub>2</sub>O<sub>3</sub>, 0.6 MgO and 0.1 Na<sub>2</sub>O. The stones for the experiments were carefully chosen to avoid stones with impurities. They were cut in the right shapes with the Micracut. The Micracut 151 is a low-speed precision cut off machine used for precise and deformation free cutting of materials. Subsequently, the samples were polished to remove any unevenness. The polishing was done by using the LaboForce-100 of Struers. The dimensions of the stones were approximately 13 x 13 x 7 mm. The samples weight was 2.12 ± 0.03 gram.

The ash was added in cavities in the stone samples. Therefore, cavities were drilled in the samples. The cavity had a diameter of 4 mm and a depth of 2 mm. Appendix B, Figure B2 shows an example of the sample with the cavity.

### 4.3 Limestone exposure

The limestone samples with ash were exposed in the tube furnace. A reference (a sample without ash), a sample with ash of wheat straw, a sample with ash of forest residues and a sample with ash of DDGS were exposed at 1100°C. After that, 4 identical samples were exposed at 1350°C. When the tube furnace had reached the set temperature, the CO<sub>2</sub> and O<sub>2</sub> flow were set at 0.11 l/min and 6 ml/min respectively. After that, there were waited for another 30 minutes in order for the tube to stabilise. Before the exposure of the samples, they were dried in 110°C for 10 minutes. The dryer removed the possible presence of moisture. After that, the samples were weighed and the cavities were filled with 10 ± 0.01 mg ash. The sample was placed in a ceramic holder (Appendix B, Figure B2) and was, using a thin glass tube, pushed to the middle of the ceramic tube of the furnace. The exposure time was 25 minutes. During the exposure, a camera made photographs of the sample in the tube. The photographs show the physical changes of the limestone during the heating. After exposure, the sample cooled down and were weighed again. The samples were stored in jars filled with nitrogen gas. It is better to fill the jars with nitrogen instead of air. Air contains moist which can affect the sample.

#### 4.4 Sample preparation for SEM analyses

To analyse the samples with the SEM/EDS microscope, it is important that the surface of the sample is flat and free from damage and contamination. The quicklime samples were casted in epoxy. The epoxy protects the sample from moisture and contamination. Alongside, the epoxy casts the sample in the right template for the SEM analysis.

As mentioned, it is important that the surface of the sample is flat and free from damage and contamination. The epoxy sample (Appendix B, Figure B3) was polished by using the LaboForce-100 of Struers. The aim of the polishing was to reach the right height of the sample and to make a flat surface. The sample is polished up to the centre of the stone (Appendix B, Figure B4). There was effort made with a high coarseness to remove a lot of material to reach the right height. Then, it was important to polish the surface without scratches. Different disks were used with a continuous decreasing coarseness to achieve the flat surface. Afterwards, the samples were stored again in jars filled with nitrogen gas.

#### 4.5 Sample analysis

The samples were analysed with the SEM/EDS. It was important to make sure the samples were free from dirt. Therefore, the samples were cleaned with ethanol. To avoid contamination, the samples were only touched with gloves on. The samples were loaded in the microscope.

The analyses were done at a low vacuum atmosphere with the following specifications: the EP target was set on 60 Pa, the EHT at 15 kV and the I probe at 600 pA for taking images and 800 pA for using EDS.

Large area images of the samples were made in order to create a clear overview. Subsequently, different images of interesting spots were made, including the ash layer. To compare the microstructure of the several samples, images were made directly under the interface between the stone and ash with a magnification of 2000x of all the samples.

Afterwards, the samples were analysed with help of the EDS detector. The EDS is in connection with the SEM. At the SEM, an image was created after which the EDS could determine the elements in that area. The elemental analyses were done at the ash, the surface of the stone, the middle of the stone and other interesting parts. First, areas were analysed at a low magnification to create an overview. Afterwards, the magnification was increased to make more specific analyses. Additionally, the elemental composition of the pure ash of the biomasses were analysed.

##### 4.5.1 Structure analysis

With the images of the structures of the samples obtained by the SEM, a microstructure analysis was done. As a result of this analysis, it was possible to display the effect of the different ashes and temperatures on the surface structure of the quicklime.

The images were processed in the computer program ImageJ. The structure pictures were converted to binary pictures which were required for further analysis. First, the function 'Smooth' was applied, this function blurs the picture. Afterwards a local threshold 'Otsu' with a radius of 20 was applied. This function provided the best binary picture.

For the microstructure analysis, a Matlab Code was made which provides the following three results: The number of pores in the microstructure, the porosity of the microstructure in percentage and the width of each pore in the microstructure. These results are based on a method where 500 random lines, with each the same length, are drawn in the image. This code is presented in Appendix C.

Matlab gives for each line the three mentioned results. Afterwards, the results of all the lines are displayed in three histograms.

This Matlab Code is used for all the binary pictures obtained with ImageJ. Subsequently, the histograms of the pictures can be compared with each other to find the differences between the microstructures.

## 4.6 Risk analysis

During practical work, there were a few safety risks. The risks were known before the practical work started. In this subsection, several risks will be discussed.

### 4.6.1 Hot surfaces

The kiln used for burning the biomasses was heated till 550°C. It was important to wear heat-resistant gloves when the barrels with biomass were replaced.

The tube furnace was heated until 1100°C and 1350°C. It was important that the furnace heated up and cooled down with a rate of 3°C/min. If the heating rate is too high, the ceramic tube will experience great stress and could break. During the (re)placing of the samples, it was important to wear heat-resistant gloves, safety shoes, a lab coat and safety glasses with dark glass. The safety glasses with dark glass are important because the light in the tube furnace is really bright due to the high temperature.

### 4.6.2 Reactivity quicklime

The product CaO is a reactive solid. Thermal energy is released when CaO is in contact with water. In the subsection '2.2 Quicklime', the reaction is discussed.

To prevent the CaO from coming into contact with water, all the cleaning work was done with ethanol. Beside this, a lab coat and gloves were worn during the practical work.

## 5. Results

In this section, the results of the experimental work are presented. The ash composition and infiltration are presented in several graphs. All the elemental compositions are relative and excluded from carbon, oxygen and chlorine. Carbon and oxygen are excluded because of several reasons. In the first place the epoxy, where the samples are stored in, naturally contains carbon and oxygen. For the EDS it is impossible to distinguish between the carbon and oxygen in the epoxy and in the quicklime/ash. Besides that, carbon and oxygen are relatively light elements, whereby the elemental analyses aren't that accurate. Chlorine is excluded for the reason that epoxy naturally contains chlorine, besides that, chlorine is not expected in the stone either. Besides the ash composition and infiltration, the microstructure of the quicklime is analysed. This is done with image analyses with both ImageJ and Matlab.

### 5.1 Ash composition after combustion

The ash composition of the several biomasses presented in '2.4 Combustion of biomass' is based on the theory that  $\text{CO}_2$  and  $\text{H}_2\text{O}$  will volatilise and the remaining elements will form the ash. However, it is possible that the real ash composition used with our samples differs from the ash composition based on the elemental analyses of the biomass. The EDS analyses of sample ashes determines the ash composition of the biomasses after the combustion. Figure 9 shows the comparison between the ash composition determined by the EDS with the ash composition based on the elemental composition of the biomass. Only the elements with a wt% higher than 5 wt% are presented. The darker colour represents the EDS analyses and the lighter colour the composition based on the elemental composition.

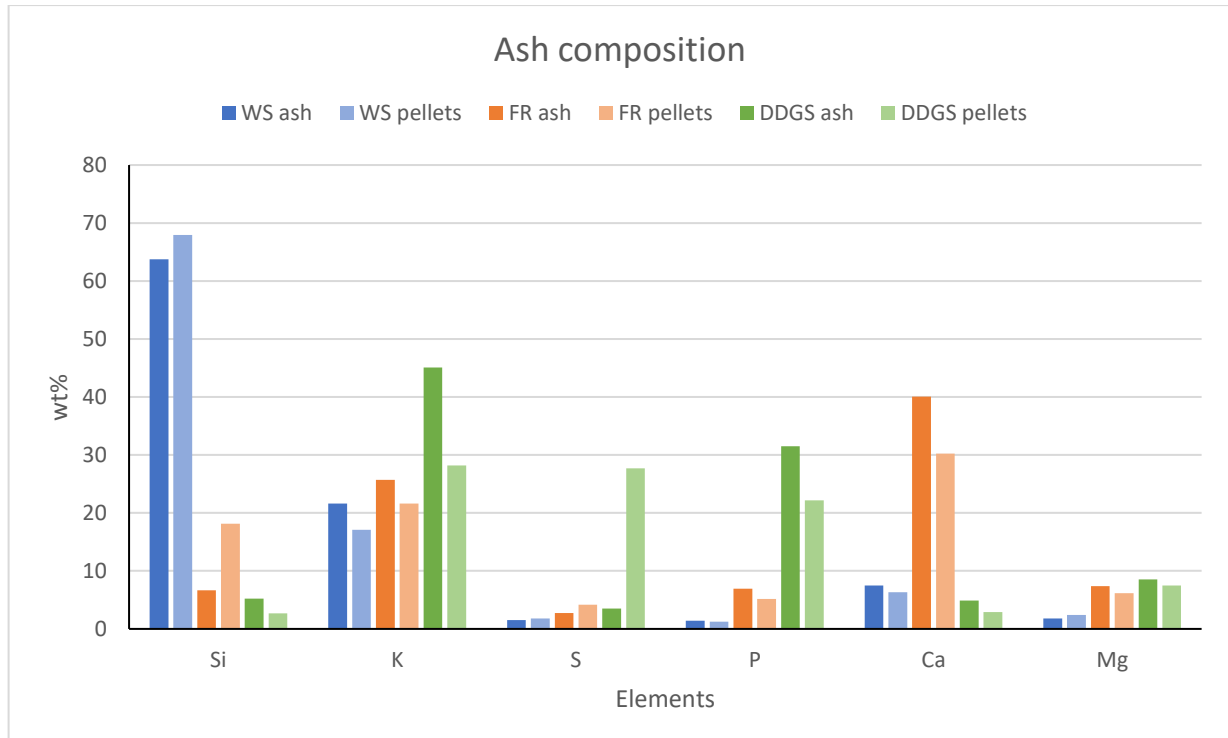


Figure 9 Relative composition of ash-forming elements of the biomass determined with the EDS (dark colours) and the ash composition based on the elemental composition of the unprepared biomass pellets (light colours).

## 5.2 Samples overview

The SEM analyses provided overall images of the samples. Figure 10 shows these overall images of the several samples at both exposure temperatures of 1100°C and 1350°C. The two reference samples, the wheat straw 1100°C and 1350°C, the forest residues 1350°C and DDGS 1350°C contain a crack. These cracks could have originated during the heating or cooling process of the stone in the furnace. Concerning the DDGS sample at 1350°C, the crack is orientated in a way that there is deep difference. That clarifies why the SEM picture can't reproduce a picture of the whole sample.

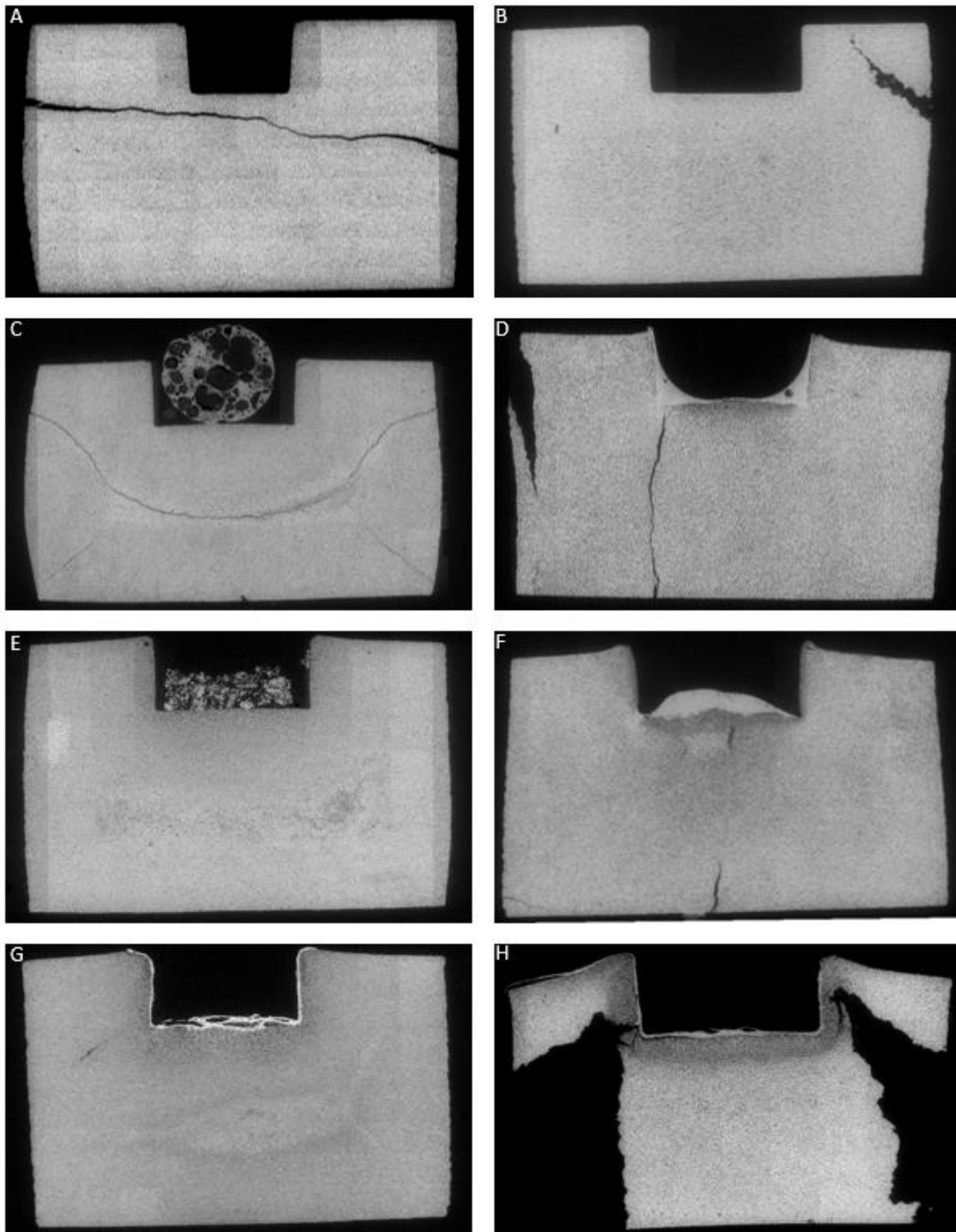


Figure 10 A: Reference 1100°C, B: Reference 1350°C, C: Wheat straw 1100°C, D: Wheat straw 1350°C, E: Forest residues 1100°C, F: Forest residues 1350°C, G: DDGS 1100°C, H: DDGS 1350°C

### 5.3 Reference

The reference quicklime samples were analysed with the EDS. At different areas, the elemental composition of the sample was determined. The theoretical composition of quicklime from pure limestone is CaO. The analyses with the EDS showed an elemental composition of 0.7 wt% magnesium, 0.2 wt% chlorine and 99.1 wt% calcium at both the 1100°C and 1350°C reference. The 0.2 wt% chlorine is due to the epoxy. As already mentioned, the chlorine is excluded in further displayed results.

### 5.4 Ash composition after exposure

After the limestone exposure to the different ashes at 1100°C and 1350°C, the composition of the (melted) ash is reformed. In this subsection, the elemental composition of the remaining ash in the cavity is presented. The elemental composition is determined with the EDS. For each sample, 4 to 5 analyses were done at the ash. For each analysis, the program AZtec (which is in cooperation with the EDS) displayed the elemental composition and figures with the elemental distribution in the ash and stone. Figure 11 displays an example of one of the analyses. The analysis is of the left upper corner of the wheat straw 1100°C sample. Figure 11A shows the original image of the spot the EDS has analysed. Figure 11B up to Figure 11F show the elemental distribution. Table 1 presents the elemental composition in wt% of that area.

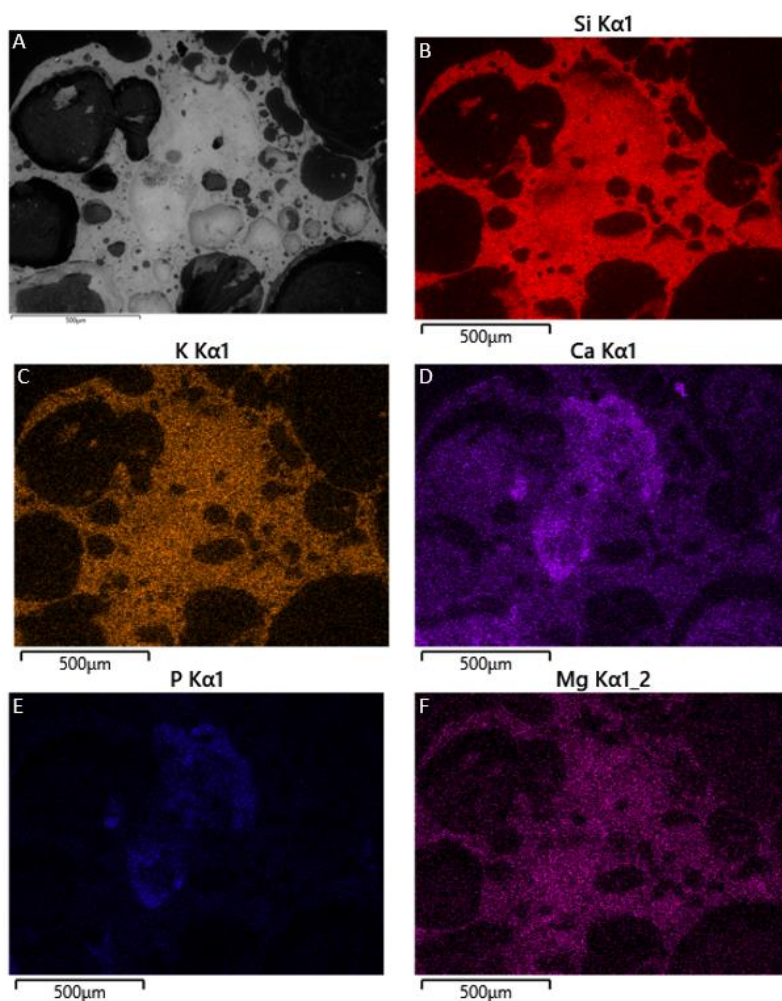


Figure 11 Elemental composition of wheat straw 1100°C left upper corner of the 'ash ball' as determined by EDS. Magnification 200x, A: Unprocessed image, B: Silicon, C: Potassium, D: Calcium, E: Phosphorus, F: Magnesium

Table 1 Elemental composition of area analysis of the left upper corner of the ash ball in the wheat straw 1100°C sample, analysed by EDS (AZtec program)

Element	wt%
Si	58.5
K	17.4
Ca	16.0
P	3.2
Mg	1.9
Na	1.0
Al	0.8
Fe	0.6
S	0.6

For each sample, 4 or 5 area analyses of the ash were done, 3 or 2 with a high magnification (2000x) and 2 with a lower magnification (200x). In Figure 12, 13 and 14, the mean ash composition of each biomass ash after exposure is presented. The black bars represent the ash composition of the pure ash analysed with the EDS. The coloured bars represent the elemental composition of the remaining ash in the cavity of the samples. In this graph, elements with a lower wt% of 1.0% are excluded.

The wheat straw ash, especially the 1350°C sample, contains a higher calcium content than the pure ash (Figure 12). The lower content of silicon and potassium is a result of the higher calcium content.

The potassium content is in both the forest residue 1100°C and 1350°C much lower than the pure ash of forest residue (Figure 13). The increased calcium content may lead to an unstable position of potassium through which potassium can have volatilised during the exposure to the high temperatures [23].

Similar to the wheat straw sample, the calcium content in both the DDGS 1100°C and 1350°C samples is much higher than the calcium content in the pure DDGS ash (Figure 14).

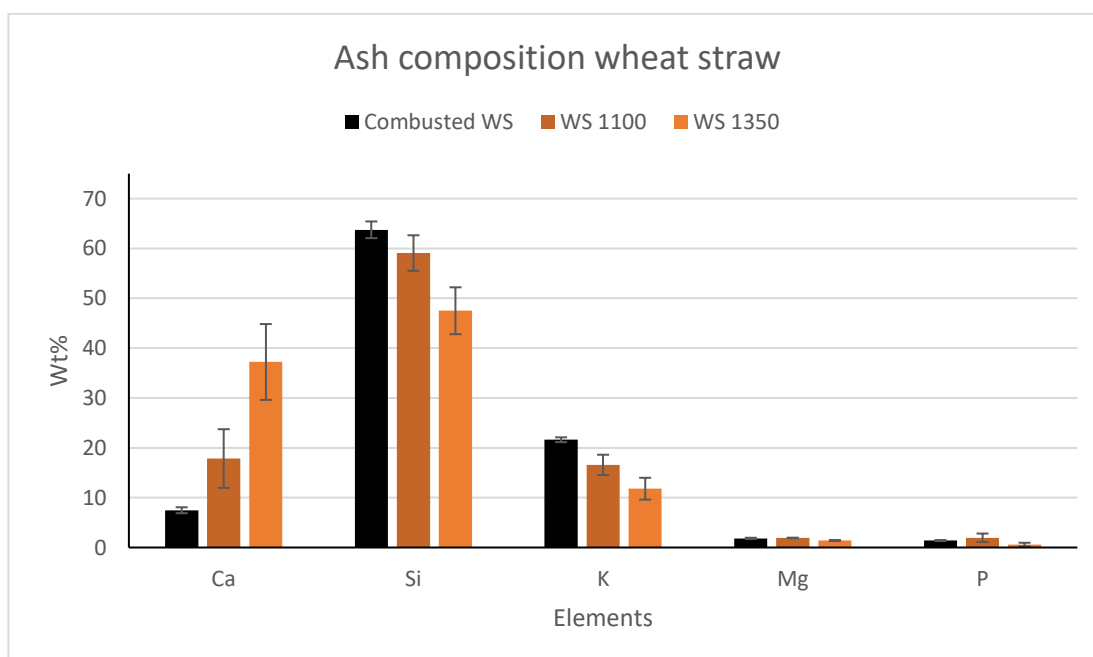


Figure 12 Relative ash composition of wheat straw. The black bars represent the ash composition of the unprocessed wheat straw ash. The coloured bars represent the ash composition of the remaining ash in the cavity after exposure

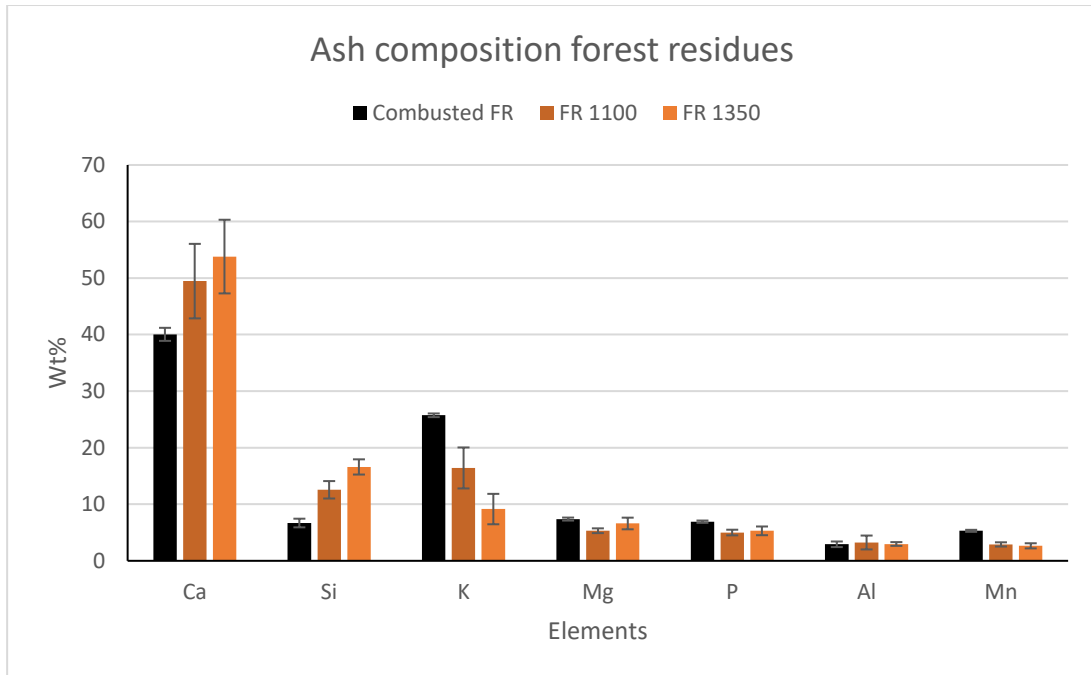


Figure 13 Relative ash composition of forest residue. The black bars represent the ash composition of the unprocessed forest residue ash. The coloured bars represent the ash composition of the remaining ash in the cavity after exposure.

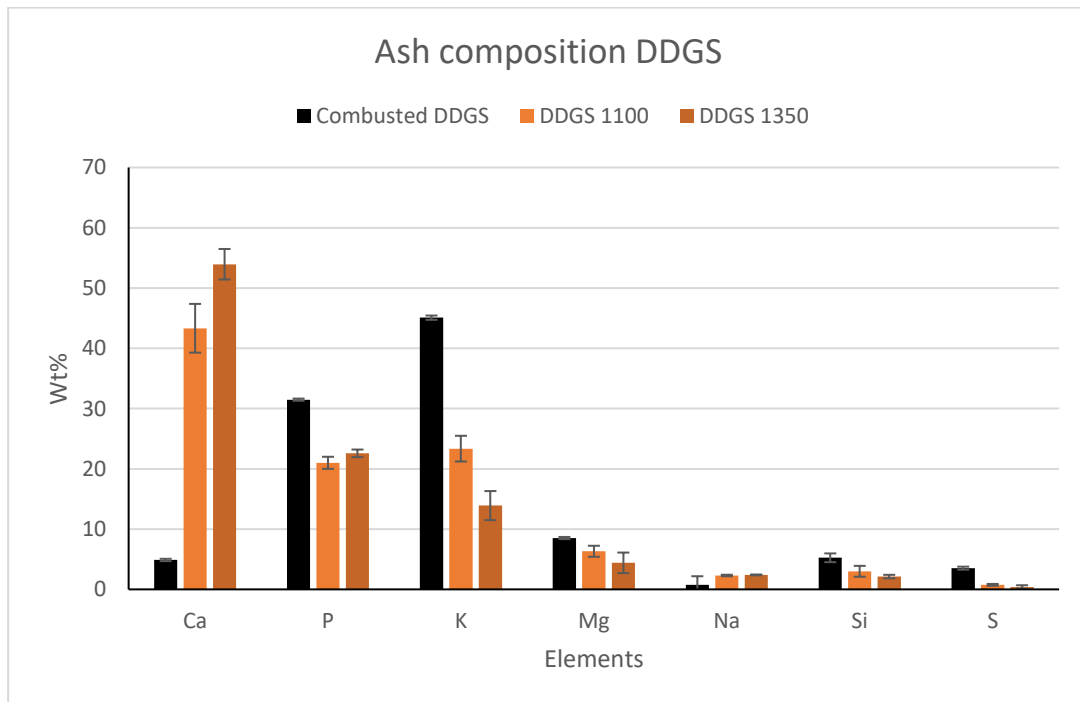


Figure 14 Relative ash composition of DDGS. The black bars represent the ash composition of the unprocessed DDGS ash. The coloured bars represent the ash composition of the remaining ash in the cavity after exposure.

## 5.5 Ash infiltration

The ash infiltration in the stone was determined by SEM/EDS analyses of 3 different areas, which are directly below each other. One area is at the edge of the stone, the second area exactly 0.1 mm underneath and the last area exactly 0.2 mm under the first area. All the analyses were done with a magnification of 2000x. Appendix B, Figure B5 shows a visual view of dimensions of the areas. Appendix B, Figure B6 shows the analysed areas of each sample. In all the graphs, calcium is excluded since the quicklime consists of CaO.

Figure 15, 16 and 17 represent the ash infiltration of the wheat straw ash in the stone during the exposure at the different temperatures. Figure 15 is an analysis of one area directly under the 'ash ball' of the wheat straw 1100°C sample. The areas besides the ash ball shows barely any infiltration of the ash. Figure 16 shows an average of two area analyses, one under the left corner and one under the right corner of the cavity, of the wheat straw 1350°C sample. The ash infiltration of the wheat straw ash in the middle of the cavity is presented Figure 17. Note, the y-axis is smaller in comparison to Figure 15 and 16.

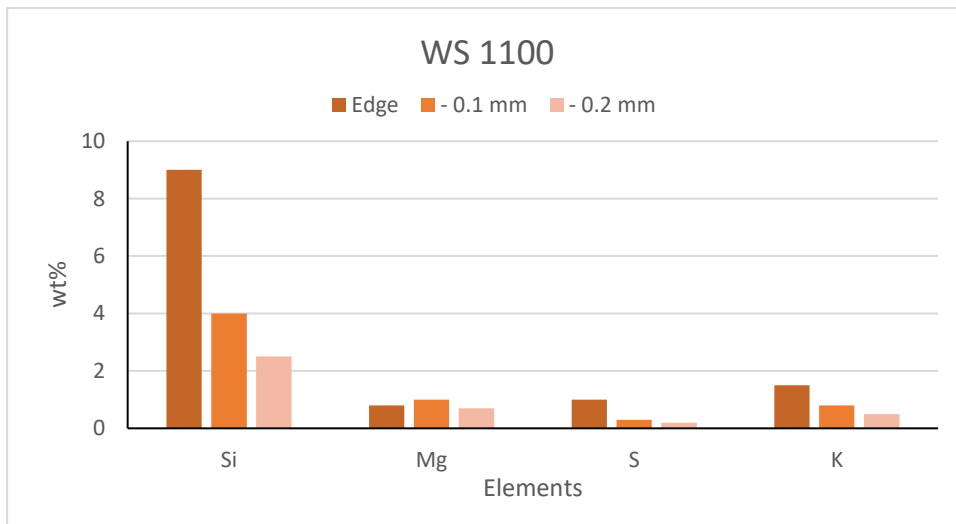


Figure 15 Ash infiltration of the wheat straw ash in the stone during the exposure at 1100°C, area 1, analysed directly under the 'ash ball'

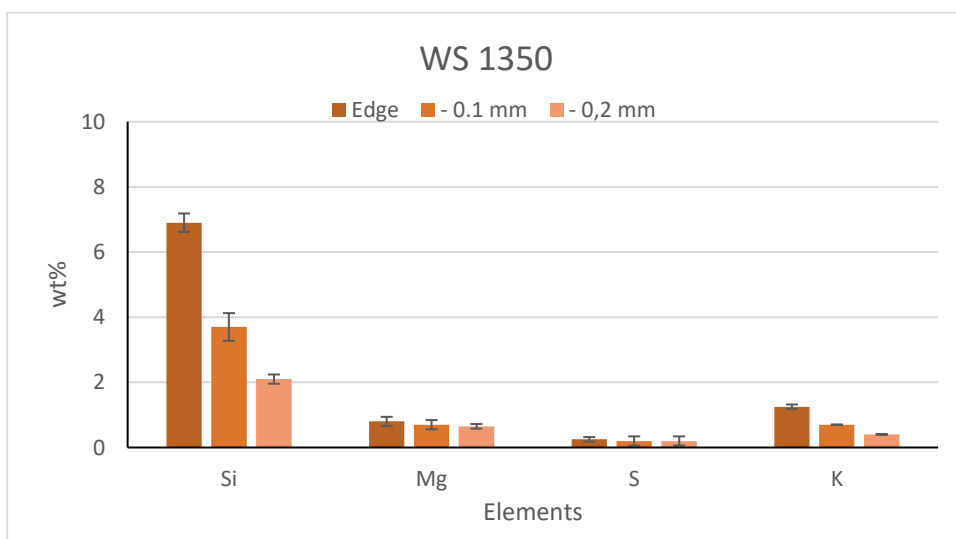


Figure 16 Ash infiltration of the wheat straw ash in the stone during the exposure at 1350°C, area 1 and 2, average of the left and right corner of the cavity

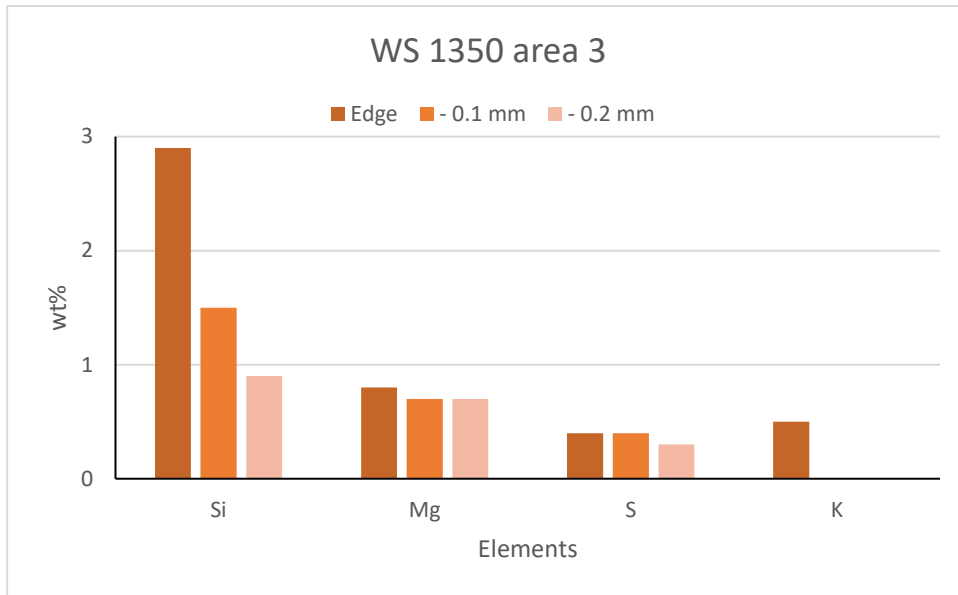


Figure 17 Ash infiltration of the wheat straw ash in the stone at the middle of the cavity during the exposure at 1350°C, area 3, analysed under the centre of the cavity

Figure 18 represents infiltration of the forest residue ash in the stone at 1100°C. The results in this graph shows an average of two area analyses. The elemental composition of the two analysed areas of the forest residue 1350°C sample differs so much that the results are separated as displayed in Figure 19 and 20.

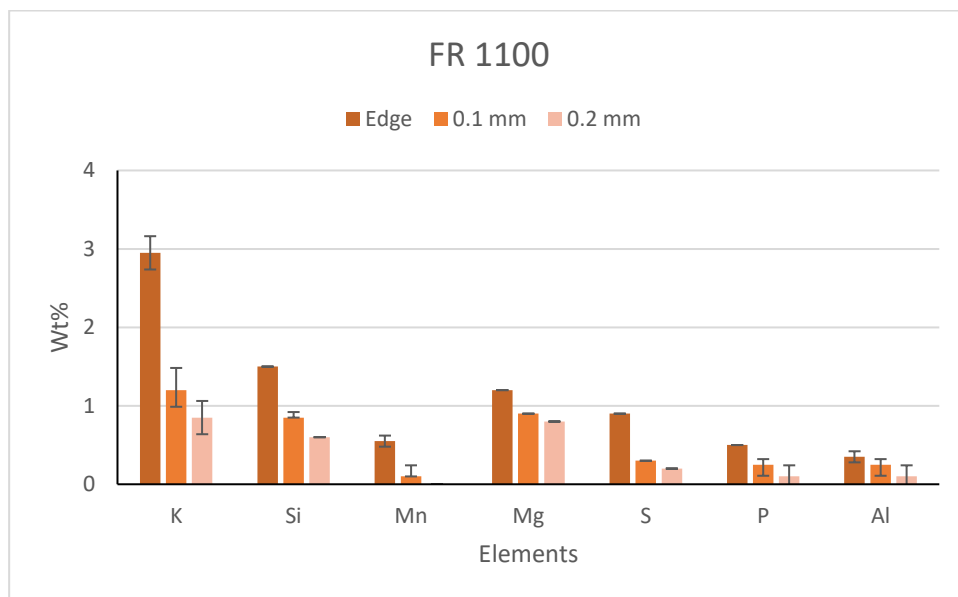


Figure 18 Ash infiltration of the forest residue ash in the stone during the exposure at 1100°C, area 1 and 2, average of two areas directly under the interface between the stone and the ash

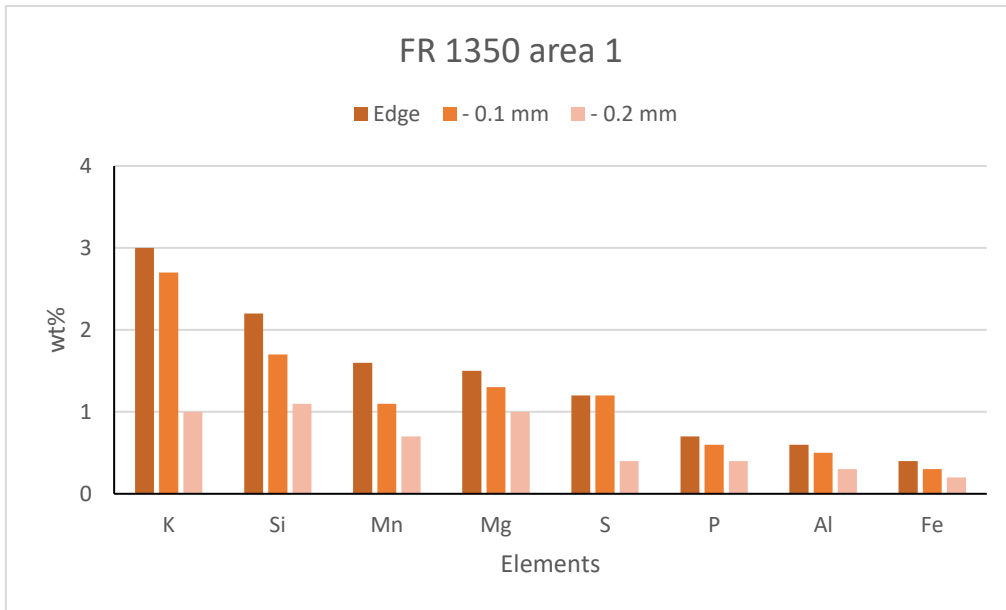


Figure 19 Ash infiltration of the forest residue ash in the stone during the exposure at 1350°C, area 1, analysed directly under the interface between the stone and the ash

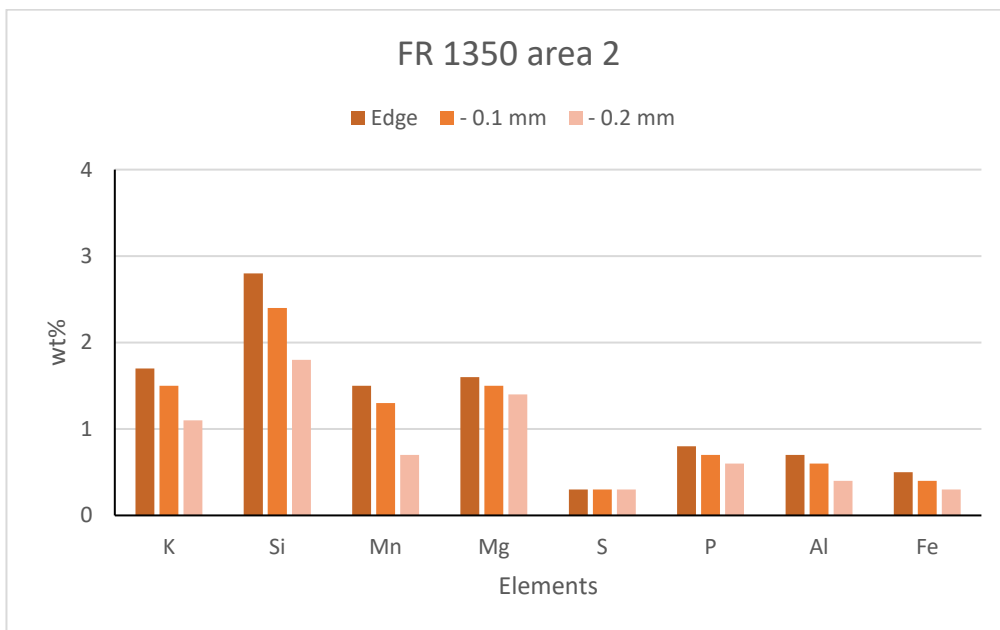


Figure 20 Ash infiltration of the forest residue ash in the stone during the exposure at 1350°C, area 2, analysed directly under the interface between the stone and the ash

Figure 21 and 22 represent the elemental composition of two areas of the DDGS' ash infiltration in the stone at an exposure temperature of 1100°C. The number of infiltrated elements varies a lot between the two areas. Figure 23 displays the ash infiltration at two areas at the exposure temperature of 1350°C. Figure 24 displays the ash infiltration of a third area of this stone. The ash infiltration of areas 1 and 2 differs significantly from area 3. Figure 25 shows the microstructure of the different areas on the edge of the stone. Area 3 has smaller grains than areas 1 and 2.

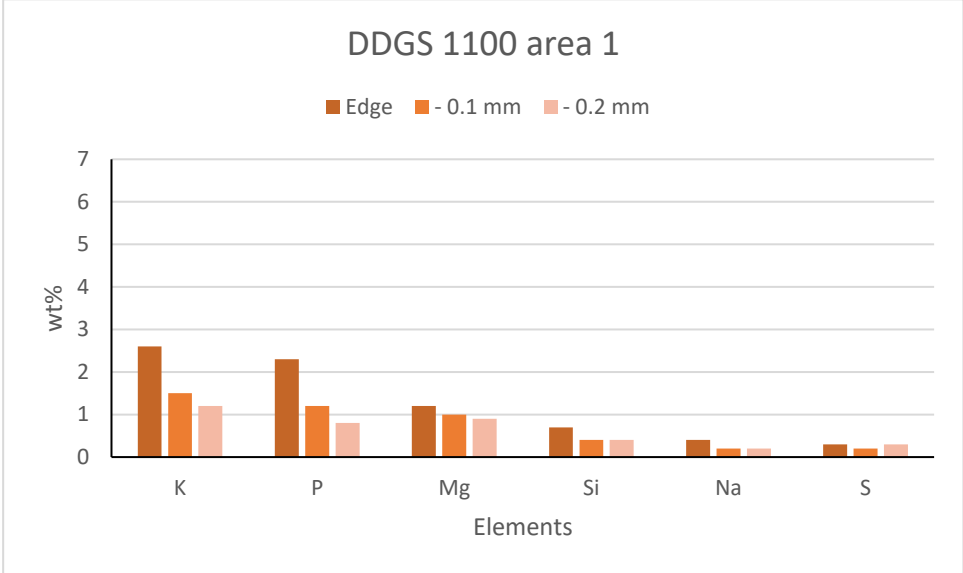


Figure 21 Ash infiltration of the DDGS ash in the stone during the exposure at 1100°C, area 1, analysed directly under the interface between the stone and the ash

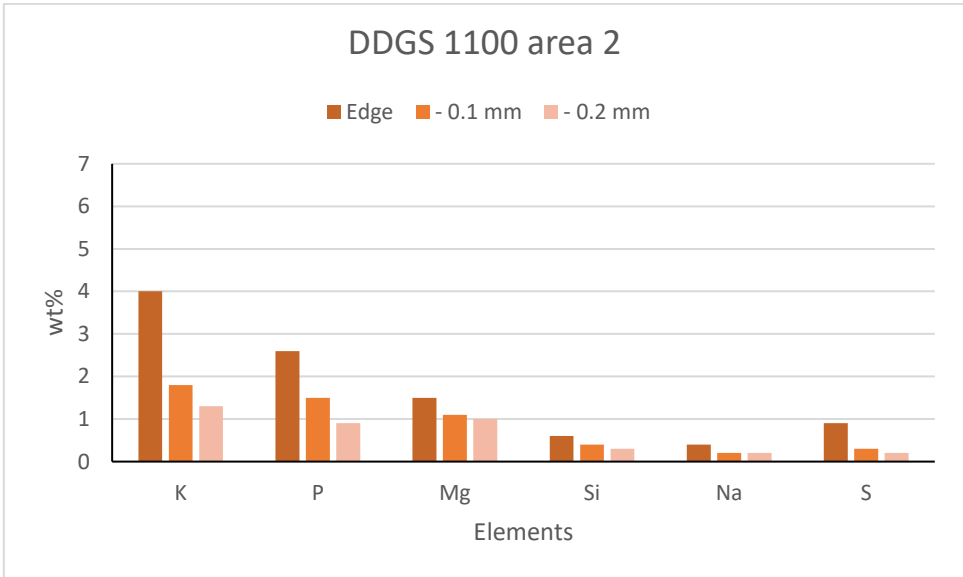


Figure 22 Ash infiltration of the DDGS ash in the stone during the exposure at 1100°C, area 2, analysed directly under the interface between the stone and the ash

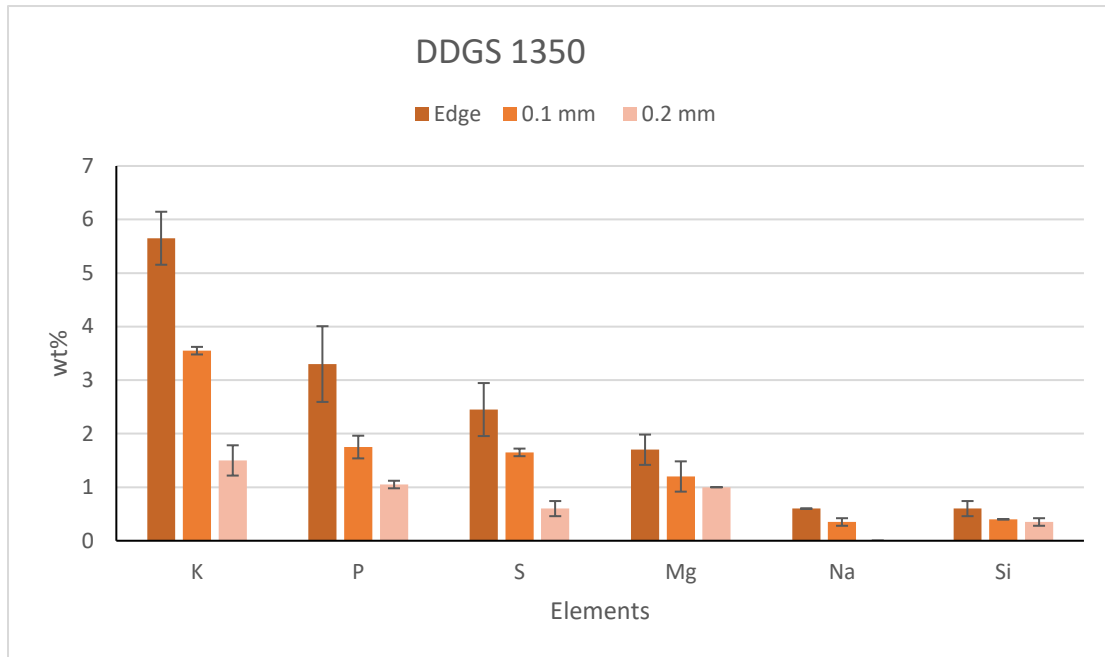


Figure 23 Ash infiltration of the DDGS ash in the stone during the exposure at 1350°C, area 1 and 2, area 1 and 2, average of two areas directly under the interface between the stone and the ash

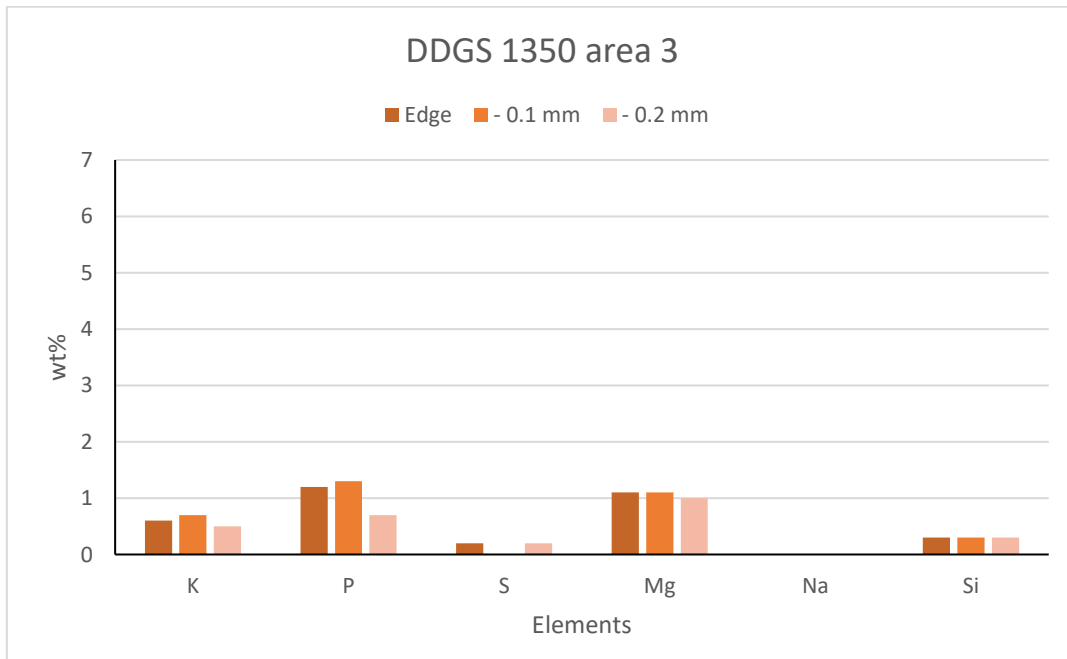


Figure 24 Ash infiltration of the DDGS ash in the stone during the exposure at 1350°C, area 3, analysed directly under the interface between the stone and the ash

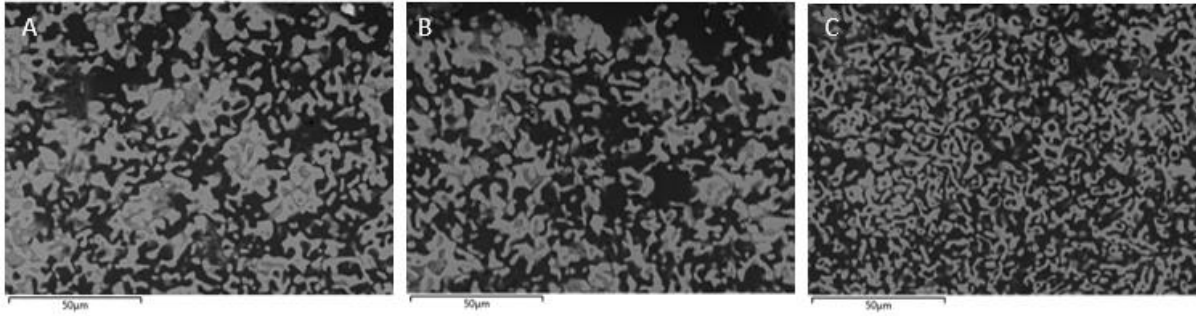


Figure 25 Structure DDGS 1350°C 2000x, A: Area 1, B: Area 2, C: Area 3

## 5.6 Structure

A microstructure analysis was done for every sample. These analyses were done with help of images of the structure of the quicklime close to the interface between the quicklime and ash. The images were obtained by the SEM. The microstructure analysis consisted of two steps. First, the images were converted to binary pictures. Afterwards, these images were analysed with the focus on the porosity, the number of pores and the pore width. In the first subsection, the conversion to the binary image (the thresholding) will be clarified. In the second subsection, the results of the structure analyses are presented.

### 5.6.1 Threshold

The programme ImageJ provides different methods to convert images to binary images. To find a qualified method for a good binary image that works for different types of structures, several functions were tested in ImageJ. The functions 'Smooth', 'Make Binary', 'Threshold' and 'Auto Local Threshold' were tested. The images in Appendix D, Figure D7-D13 show the results of the influence of the used functions on the image. All the images were critical observed and compared with the original structure image. The binary image edited with the functions 'Smooth' and 'Auto Local Threshold; Otsu; Radius 20' provided the best binary pictures for the structure images (Figure 26). This is based on the similarity of the grains and the smoothness of the binary. The white parts of the images are the grains and the black parts are the pores.

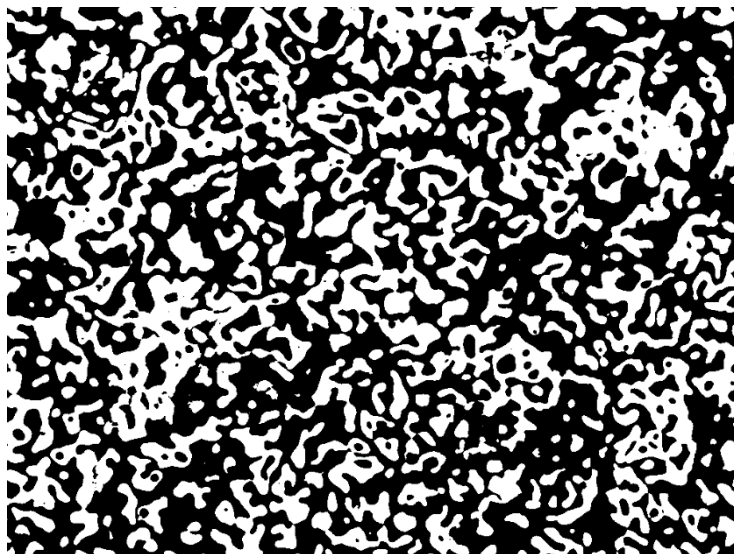


Figure 26 Structure DDGS 1350°C, magnification 2000x, edited in ImageJ: 'smooth' and 'Auto Local Threshold; Otsu; Radius 20'

### 5.6.2 Pore analysis

The pore analysis is done with help of a Matlab Code. This code provides the pore width, the number of pores at each line of 10  $\mu\text{m}$ , the total porosity and the porosity at each line of 10  $\mu\text{m}$ .

The pore width is the distance between two grains. In the images, the pores are the black parts. The number of pores is given for each line of 10  $\mu\text{m}$ . This result says nothing about the number of grains in the whole picture. However, all the images are analysed with the same amount and length of lines. Because of that, all the results of the histograms can be compared with each other. The total porosity is the ratio of pore surface in the image to the surface of the whole image. The porosity at each line is the ratio of the pore surface of the line to the surface of the whole line.

Appendix E, Figure E14-E21, shows the original picture, the binary picture, the picture with the 500 drawn lines and the three histograms of each sample. Figures 27 till 29 summarise these results. Figure 27 displays the mean value of the number of pores at the lines in the images. Figure 28 displays the total porosity of each image and Figure 29 shows the pore width of all the pores at each line. The graph is cut-off at a width of 10  $\mu\text{m}$  to make the graph more readable. The pores bigger than 10  $\mu\text{m}$  occur with a frequency of lower than 0,25%. The biggest pores of wheat straw 1350°C, forest residues 1350°C, DDGS 1100°C and DDGS 1350°C are 30  $\mu\text{m}$ . The biggest pore of forest residue 1100°C is 25  $\mu\text{m}$ , of wheat straw 1100°C is 10  $\mu\text{m}$  and of the reference 1100°C and 1350°C 13,5  $\mu\text{m}$ .

The total porosity, in combination with the pore width, gives a good overview of the structure of the relevant sample. The total porosity gives the ratio of the pores, whereby the pore width analysis gives an idea of the size of the pores.

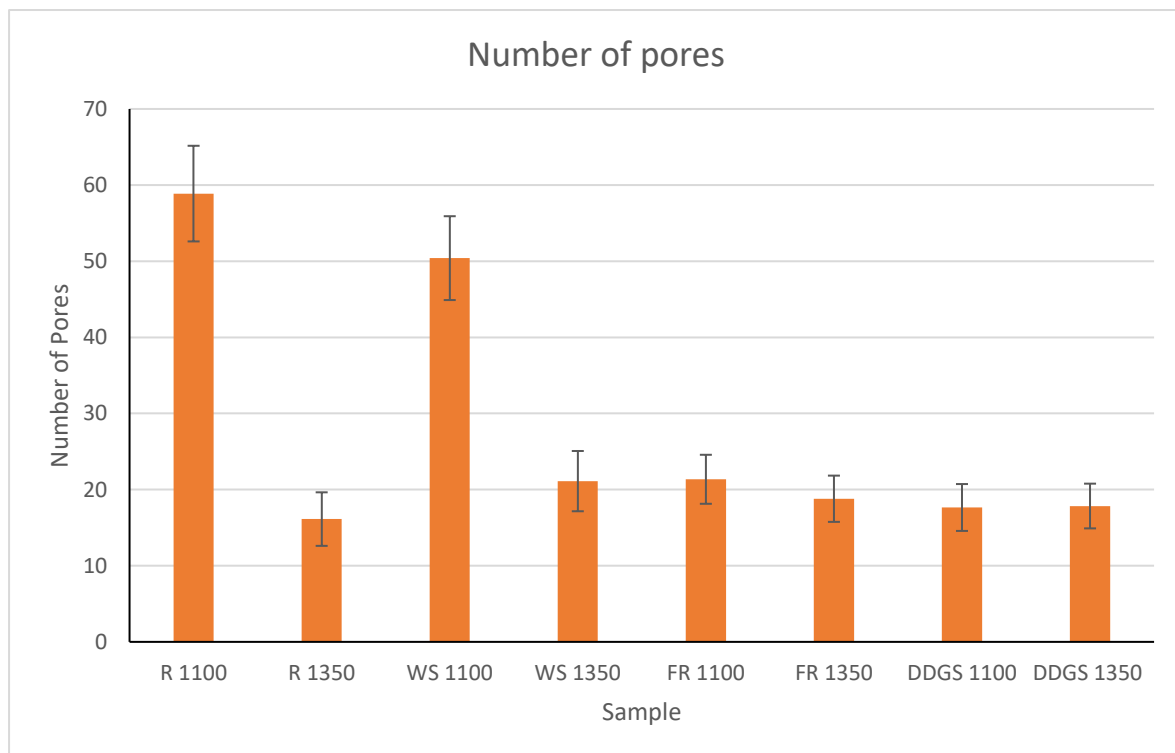


Figure 27 The mean values of the number of pores at each line drawn in the structure images

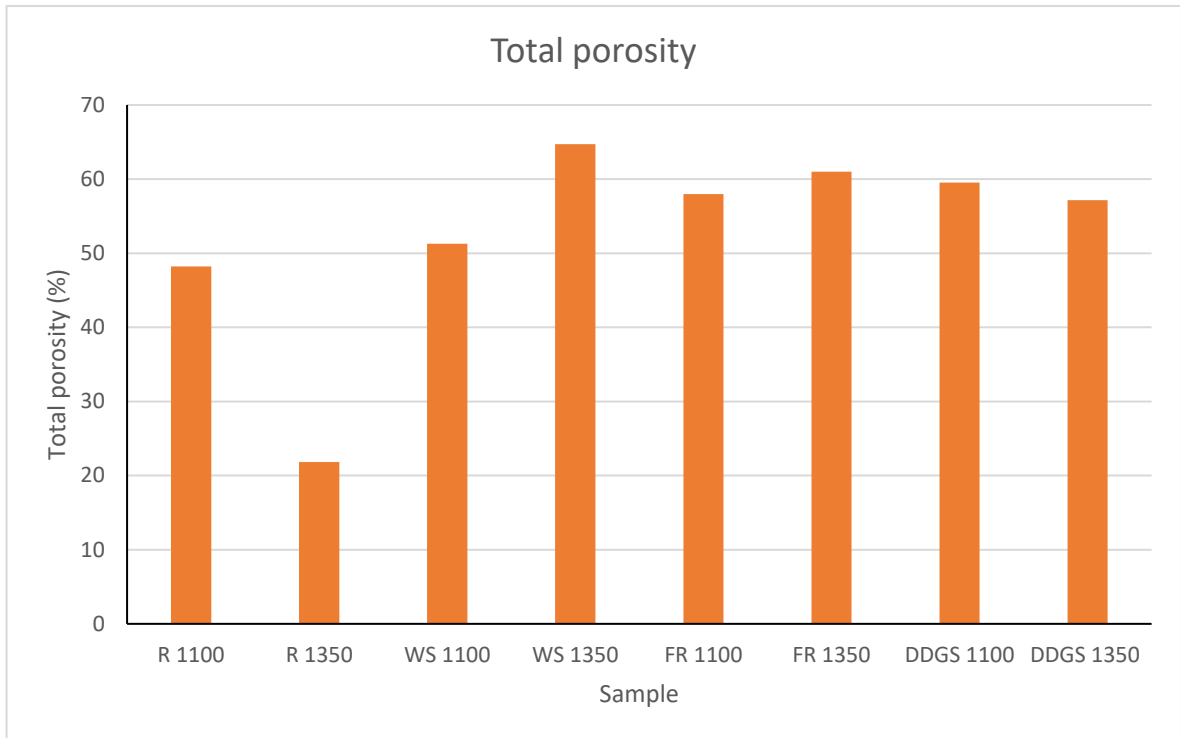


Figure 28 The total porosity of the quicklime structure determined with the structure images

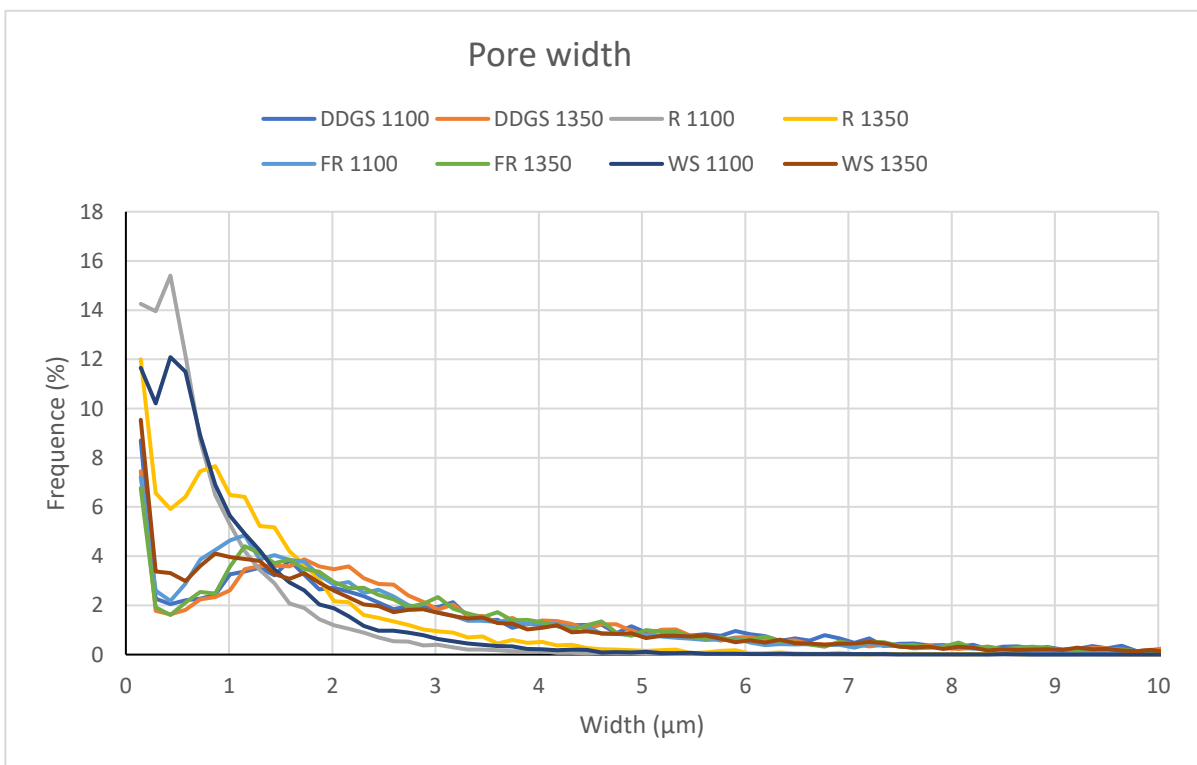


Figure 29 The pore width of each pore at the lines drawn in the structure images

## 6. Discussion

During this study, the interaction between the ashes from the biomasses wheat straw, forest residues and DDGS, and limestone during calcination is tested in a tube furnace. The ashes were tested at both 1100°C and 1350°C. The ash infiltration, changes in microstructure and reaction of ash forming elements in the exposed material were analysed with the SEM/EDS. Afterwards, the microstructures were analysed with the programmes ImageJ and Matlab.

### 6.1 Results from experimental work

During practical work, every biomass is tested at both 1100°C and 1350°C, however these were single experiments, every biomass and temperature is tested only once. Experiments with double or triple experiments alienate randomness, in this case randomness could have happened.

The reference is done to verify how the limestone sample will react at both 1100°C and 1350°C. Besides that, with help of the EDS analyses of the reference sample, it could be analysed which elements in the quicklime were natural, or which were coming from the biomass ash.

The analyses of the ash composition done with the EDS doesn't correspond totally with the elemental composition of the ash based on the elemental composition of the unprepared biomass pellets, which is based on the theory that CO<sub>2</sub> and H<sub>2</sub>O will volatilise and the remaining elements will form the ash (Figure 9). Concerning the DDGS ash, the sulphur content is frequently lower. As expected, the sulphur vaporised as SO<sub>3</sub> (g) or SO<sub>2</sub> (g) during the combustion of the biomasses at 550°C [16]. Furthermore, the forest residues' ash shows a lower silicon content. The reason for this could be the heterogeneous character of the mixture of the biomass. The wheat straw ash doesn't show unexpected differences in the ash composition.

#### 6.1.1 Wheat straw

The quicklime samples, which were exposed to the wheat straw ash at 1100°C and 1350°C, show a significant difference (Figure 10 C and D). The ash exposed at 1100°C has formed a solid ball, which is in contrast with the ash in the 1350°C sample, where the ash has flowed to the corners of the cavity and stuck to the edges of the cavity.

The ash ball in the 1100°C sample contains a lower calcium content than the 1350°C sample (Figure 12). Apparently, it was easier for the calcium to react with the elements in the ash when the ash is formed as an ash layer at the bottom of the cavity, due to the larger contact area. The high calcium, silicon and potassium content in the ash could indicate the expected K-Ca-silicate [16]. Since the potassium content is quite low in comparison with the calcium and silicon, the remaining silicon and calcium could have reacted as CaSiO<sub>3</sub> in the ash.

Moreover, ash infiltration in the quicklime is found in both the 1100°C and 1350°C samples (Figure 15, 16 and 17). Again, the elements potassium, calcium and silicon are present, which indicate a K-Ca-Silicate and probably Ca<sub>2</sub>SiO<sub>4</sub> in the quicklime [25]. The 1350°C sample has a higher concentration of ash infiltration in the corners of the cavity, where there is a thicker ash layer than in the middle, where there is only a thin ash layer. This, and the knowledge that under the ash ball of the 1100°C sample it was a lot of ash infiltration, could indicate that a thicker ash layer has a positive influence on the ash infiltration.

#### 6.1.2 Forest residues

The forest residues ash at the quicklime samples, which were exposed at 1100°C and 1350°C, reacted both differently (Figure 10 E and F). It is obvious that the ash at 1350°C has melted. This is in contrast with the 1100°C, whereby the ash looks more heterogenic and grainy.

In the ash, the 1350°C sample has a lower potassium and a higher calcium content than the 1100°C sample (Figure 13). This can indicate more potassium infiltration in the stone, or that the potassium has volatilised. The higher calcium content can indicate more calcium interaction from the stone with the ash. The relative increase of silicon in the graph is due to the changes in the potassium and calcium content.

Both samples at 1100°C and 1350°C have an ash infiltration of mostly potassium, silicon, magnesium and manganese (Figure 18, 19 and 20). However, the ash infiltration is significantly lower than in the wheat straw sample. A reason for this could be that the K-Ca-Silicate is already formed in high amounts in the ash, instead of in the stone. In the forest residues samples, this is more likely than in the wheat straw sample, due to the higher calcium content in the ash. Besides that, especially in the 1350°C sample, manganese and magnesium have also infiltrated. This wasn't expected, because manganese and magnesium are only present in low concentrations in the ash. Nevertheless, the magnesium could indicate a calcium-magnesium-silicate and the manganese a calcium-manganese oxide. Finally, the forest residues 1350°C sample shows at different spots at the edge of the stone, a different ash infiltration. This could be due to the heterogeneous character of the mixture of the biomass.

### 6.1.3 DDGS

The DDGS samples have both a thin ash layer at the bottom of the cavity and ash at the edges (Figures 10 G and H). One of the possible scenarios is that during the exposure, the ash melted really fast, through which it stuck to the edges. The 1350°C ash displays a dark area under the cavity of the stone. EDS analyses didn't show a different ash composition. However, all the 1350°C samples exposed with ash show a darker area under the cavity (Figure 10 D, F, H). Since the reference sample doesn't show a darker area, it is plausible that the darker areas are due to a combination of the heat and the ash.

The calcium content in the ash after exposure is significantly higher than of the pure ash (Figure 14). Because of the thin ash layer, it could be easier for the calcium of the stone to react in the ash. Also, the phosphorus didn't behave as expected. The expectation was that, due to the increased relative calcium content, the other elements would decrease. However, the phosphorus of both samples was nearly the same. A reason for this could be that phosphorus is really attracted to calcium and stayed in the ash layer together with calcium.

The ash infiltration in the stone shows a lot of variation (Figures 21-24). All spots consists mainly potassium and phosphorus, but in different quantities. The 1350°C sample has also infiltration of sulphur. The infiltrated potassium and phosphorus could indicate the orthophosphate  $\text{CaKPO}_4$ , this could be a solid or liquid. It was expected that orthophosphate could react according to reaction 10, whereby  $\text{Ca}_3(\text{PO}_4)_2$  is formed and potassium would volatilise, however, the potassium is still present. Perhaps, potassium is still too attracted to phosphorus whereby it didn't volatilise. Reaction 6 describes a reaction which could happen with sulphur and calcium. The 1350°C has sulphur infiltration, however it is unlikely that  $\text{CaSO}_4$  is formed, because this is only stable till 1200°C.

## 6.2 Structure analysis

For all binary pictures the functions 'Smooth' and 'Auto Local Threshold; Otsu; Radius 20' are used in ImageJ. On basis of a few pictures this binary method is selected. However, every picture is different. This means that for every picture another binary method is ideal. Since one binary method is chosen, it is possible that it isn't the optimal binary for every picture. This could lead to an inaccuracy in the results.

The porosity of the structure images is approached with two methods. The first method provides the total porosity of the whole image. This is calculated by dividing the black pixels by the total number of pixels. The other method provides the porosity at each line. In the results, only the total porosity is presented (Figure 28). This was valid because the mean of all the porosity values of the lines is equal to the calculated total porosity. This indicates that the method to determine the porosity is valid. The width of the porosity histograms gives the homogeneity of the structure (Appendix E Figure E14-E21). A broad histogram is equal to a high distribution in the values, which indicate a various distributed structure.

All the structures contain a high number of pores with a width of 0.144  $\mu\text{m}$ , this is equal to 1 pixel in the image (Figure 29). It is important to know that this doesn't have to correspond to a pore of 1 pixel. The pore could have a rectangle shape where the line crossed the long side of the pore. A graph with a steep decreasing line, such as the wheat straw 1100°C and the reference 1100°C, indicates mostly small pores, and some bigger pores. If the graph is less steep, such as all the other samples, it indicates that the pores are bigger, and that there is more distribution in the pore size.

According to the results of the structure analyses, the reference samples and the wheat straw 1100°C differs from the other structures (Figure 27-29). The structures of the forest residues samples, the DDGS samples and the wheat straw 1350°C all have, in proportion to the reference and wheat straw 1100°C sample, a low number of pores, a high porosity and large pores. Besides that, these samples are less homogenous. The reference 1100°C and wheat straw 1100°C both have a high number of pores, an average porosity, small pores and a higher homogeneity. The reference 1350°C deviates the most from all the other structures. This one has a low number of pores, a low porosity, small pores and a moderate homogeneity.

The structure images are all taken of the quicklime under the interface between the quicklime and ash. The samples which were exposed to ash show different results than the reference sample. This could indicate that the ash or ash infiltration affects the microstructure of the quicklime. All the samples exposed with ash have a comparable microstructure, only the wheat straw 1100°C deviates, this one behaves more like the reference 1100°C. The wheat straw 1100°C sample is the sample where the ash has formed an 'ash ball'. At the interface, besides the ash ball, barely ash infiltration was found. A clarification of the similarity with the reference 1100°C is that the image is taken at one of the sides of the cavity, where no or barely ash has infiltrated. Even the temperature of the furnace expresses no difference in microstructure for the biomasses forest residues and DDGS. This contradicts the physical change during the exposure. Since the quicklime samples, which were exposed at 1350°C, shrank significant more than the 1100°C samples.

Moreover, in the reference samples, there is no ash that could affect the microstructure, it can behave naturally. The reference samples indicate that the temperature affects the microstructure. If all the samples would also be analysed further down in the stone, where the ash can't affect the microstructure, the case could be that the microstructures behaved more as the reference.

## 7. Conclusion

The purpose of the study was to analyse how different ashes from the biomasses wheat straw, forest residues and DDGS affect the product quality of quicklime. The effect of the ash was tested by using a tube furnace where the limestone and the ash from the biomasses were exposed at 1100°C and 1350°C.

In all the samples, the ash of the biomass has infiltrated in the quicklime. The wheat straw samples have the most infiltration, but only underneath the ash layer. In case of the wheat straw 1100°C sample, underneath the sides of the 'ash ball' barely ash infiltration was found. The DDGS had the second most ash infiltration and the forest residues samples had the least ash infiltration. In both the wheat straw and forest residues, K, Ca and Si was found, possibly in the form of K-Ca-silicates. In the wheat straw samples, it is possible that the K-Ca-silicate is formed in both the ash layer and interface of the quicklime, whereas in the forest residues the possible K-Ca-silicate is mainly formed in the ash layer. Due to the heterogenous character of the forest residues, both the ash composition and ash infiltration is not identical at different spots in the sample. The DDGS samples prove that calcium and phosphorus is attracted to each other. Besides phosphorus, potassium has also infiltrated.

The microstructure analyses verify that the ash of the biomass affects the microstructure of the quicklime at the interface. In comparison with the reference samples, the quicklime samples exposed with biomass ash have a higher porosity at the interface. In these samples, there is no visible difference between the 1100°C and the 1350°C quicklime samples. This is in contrast with the reference samples, whose structures differ significantly at the different temperatures.

A proposal which biomass should be the best option to substitute coal as fuel in the heating process of the quicklime manufacturing, can't be made. For that more analyses are needed. Nevertheless, it can be concluded that all tested biomasses affect the microstructure at the interface of the quicklime samples, and the ash of the biomasses infiltrates at the interface of the quicklime and interactions between elements occurs.

## 8. Recommendations

If more confirmation is needed, it could be valuable to accomplish a duplicate test to exclude randomness. Besides that, it could be recommended to analyse more areas of the microstructure of the quicklime samples, such as areas at different depths into the stone. In this research, only the microstructure of one area at the interface is analysed.

Furthermore, in this research, the reaction between the biomass ash and the quicklime is forced by putting the ash directly at the surface of the limestone sample. It could be valuable to do further studies to evaluate how the different fuels would affect the product quality and process performance in industrial scale.

Only the possible ash infiltration of the biomass in the quicklime and the possible changes in the microstructure at the interface were analysed. These are two points that describe the influence of the biomass ash at the product quality. To provide more knowledge about the influence of the biomass ash on the quicklime, it can be recommended to analyse other quality characteristics, such as the reactivity of the quicklime and the compression strength.

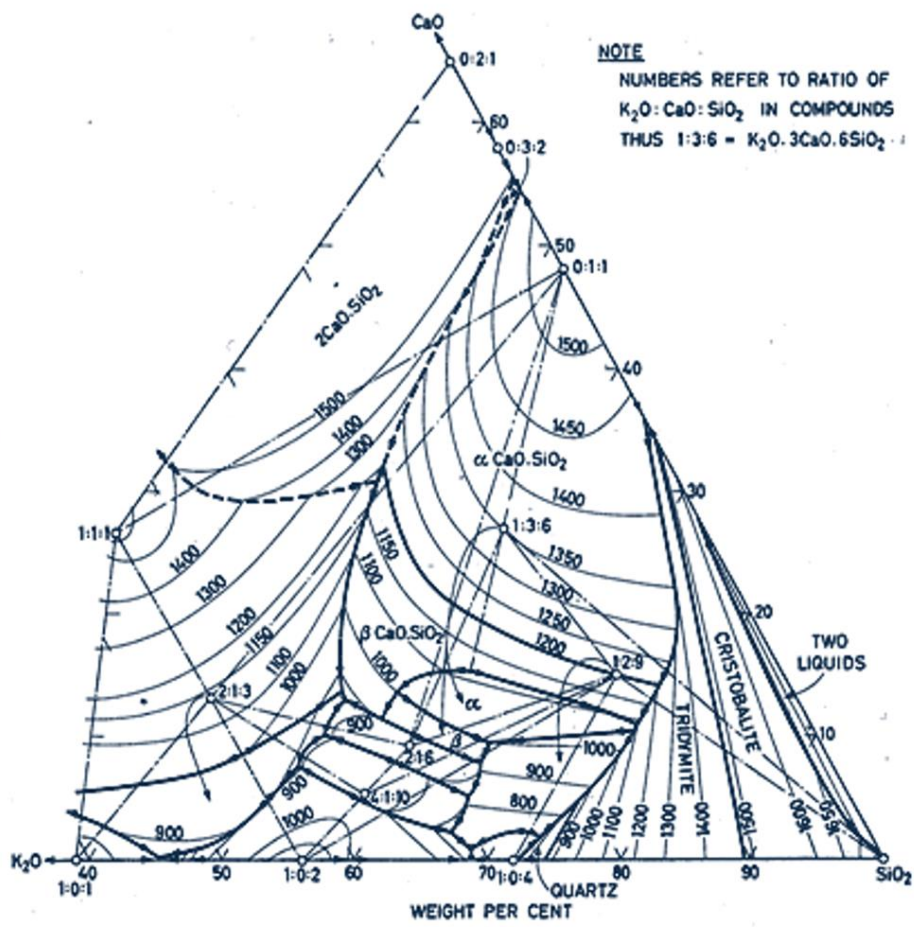
The final recommendation is to test more biomasses with limestone to find the perfect substitute for coal as fuel in the heating process of the quicklime manufacturing.

## 9. Reference list

- [1] R. C. Selley, "Limestones," 2005.
- [2] P. Ciullo, *Industrial minerals and their uses: a handbook and formulary*, 1st ed. William Andrew, 1996.
- [3] M. Eriksson, "Sustainability measures in quicklime and cement clinker production," Umeå University, 2015.
- [4] D. J. Harrison, "Industrial Minerals Laboratory Manual - Limestone," *Br. Geol. Surv.*, vol. WG/92/29, no. Mineralogy and Petrology Series, p. 54, 1992.
- [5] H. King, "Limestone: Rock Uses, Formation, Composition, Pictures." [Online]. Available: <https://geology.com/rocks/limestone.shtml>. [Accessed: 16-Nov-2020].
- [6] F. Schorcht, I. Kourti, B. M. Scalet, S. Roudier, and L. D. Sancho, *Best Available Techniques (BAT) Reference Document for the Production of Cement, Lime and Magnesium Oxide*. 2013.
- [7] K. S. P. Karunadasa, C. H. Manoratne, H. M. T. G. A. Pitawala, and R. M. G. Rajapakse, "Thermal decomposition of calcium carbonate (calcite polymorph) as examined by in-situ high-temperature X-ray powder diffraction," *J. Phys. Chem. Solids*, vol. 134, pp. 21–28, Nov. 2019.
- [8] J.-M. Commandre, S. Salvador, A. Nzihou, J. Commandré, S. Salvador, and A. Nzihou, "Reactivity of laboratory and industrial limes," *Chem. Eng. Res. Des.*, vol. 85, no. 4, pp. 473–480, 2007.
- [9] M. Eriksson, "Characterization of kiln feed limestone by dynamic heating rate thermogravimetry," *Int. J. Miner. Process.*, vol. 147, pp. 31–42, Feb. 2016.
- [10] D. Sietske Boschma, I. Kees, and W. Kwant, "Netherlands Programmes Sustainable Biomass," 2013.
- [11] R. Marks-Bielska, S. Bielski, A. Novikova, and K. Romaneckas, "Straw stocks as a source of renewable energy. A case study of a district in Poland," *Sustain.*, vol. 11, no. 17, pp. 1–18, 2019.
- [12] N. Belyakov, "Bioenergy," in *Sustainable Power Generation*, Academic Press, 2019, pp. 461–474.
- [13] S. Alanya, "WASTE TO WISDOM: UTILIZING FOREST RESIDUES FOR THE PRODUCTION OF BIOENERGY AND BIOBASED PRODUCTS FINAL REPORT," 2018.
- [14] G. Eriksson, A. Grimm, N. Skoglund, D. Boström, and M. Öhman, "Combustion and fuel characterisation of wheat distillers dried grain with solubles (DDGS) and possible combustion applications," *Fuel*, vol. 102, pp. 208–220, 2012.
- [15] M. Mandø, "Direct combustion of biomass," in *Biomass Combustion Science, Technology and Engineering*, Elsevier Inc., 2013, pp. 61–83.
- [16] D. Boström *et al.*, "Ash transformation chemistry during combustion of biomass," *Energy and Fuels*, vol. 26, no. 1, pp. 85–93, 2012.
- [17] T. N. Adams, "Lime kiln principles and operations," 2007.
- [18] Carbolite, "Universal tube furnace." [Online]. Available: [https://www.wolflabs.co.uk/document/Carbolite\\_furnaces\\_STF\\_TZF-15\\_TZF-16.pdf](https://www.wolflabs.co.uk/document/Carbolite_furnaces_STF_TZF-15_TZF-16.pdf). [Accessed: 17-Nov-2020].

- [19] C. Woodford, "How do electron microscopes work?" [Online]. Available: <https://www.explainthatstuff.com/electronmicroscopes.html>. [Accessed: 09-Dec-2020].
- [20] L. Sandblad, "Welcome to Umeå Core Facility for Electron Microscopy."
- [21] Mee, "Energy Dispersive X-Ray Spectroscopy." [Online]. Available: <https://www.mee-inc.com/hamm/energy-dispersive-x-ray-spectroscopy/>. [Accessed: 10-Dec-2020].
- [22] J. Atteberry, "The Key Components of a Scanning Electron Microscope." [Online]. Available: <https://science.howstuffworks.com/scanning-electron-microscope2.htm>. [Accessed: 09-Dec-2020].
- [23] P. Thy, C. E. Lesher, and B. M. Jenkins, "Experimental determination of high-temperature elemental losses from biomass slag," *Fuel*, vol. 79, no. 6, pp. 693–700, 2000.
- [24] N. Skoglund, "Ash chemistry and fuel design focusing on combustion of phosphorus-rich biomass," Umeå University, 2014.
- [25] B. Hokfors, "Phase Chemistry in Process Models for Cement Clinker and Lime Production," *Dep. Appl. Phys. Electron.*, vol. 87, no. 9, pp. 1–76, 2014.
- [26] "Lime (material) - Wikipedia." [Online]. Available: [https://en.wikipedia.org/wiki/Lime\\_\(material\)](https://en.wikipedia.org/wiki/Lime_(material)). [Accessed: 06-Apr-2021].

# Appendix A



Roedder, E.: Silicate melt systems. Phys. Chem. Earth 3, 224-297 (1959)

Figure A1 Ternary phase diagram of the SiO<sub>2</sub>-K<sub>2</sub>O-CaO system

Appendix B



Figure B2 Sample in ceramic holder

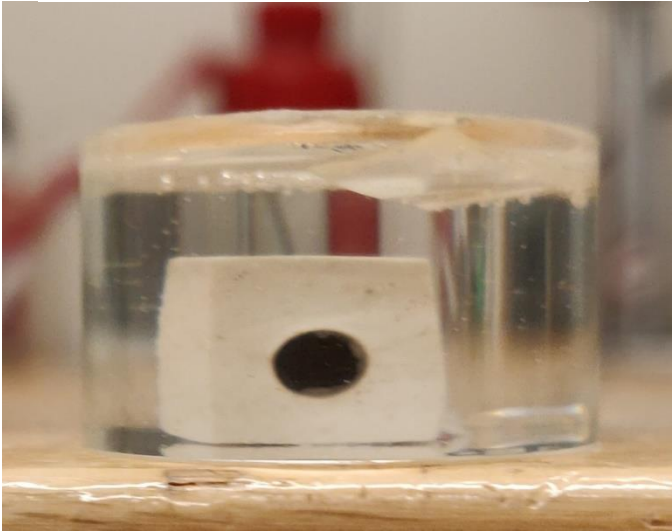


Figure B3 Sample in epoxy

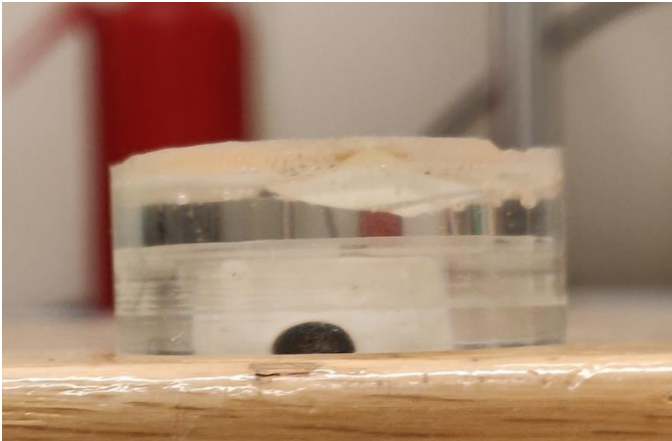
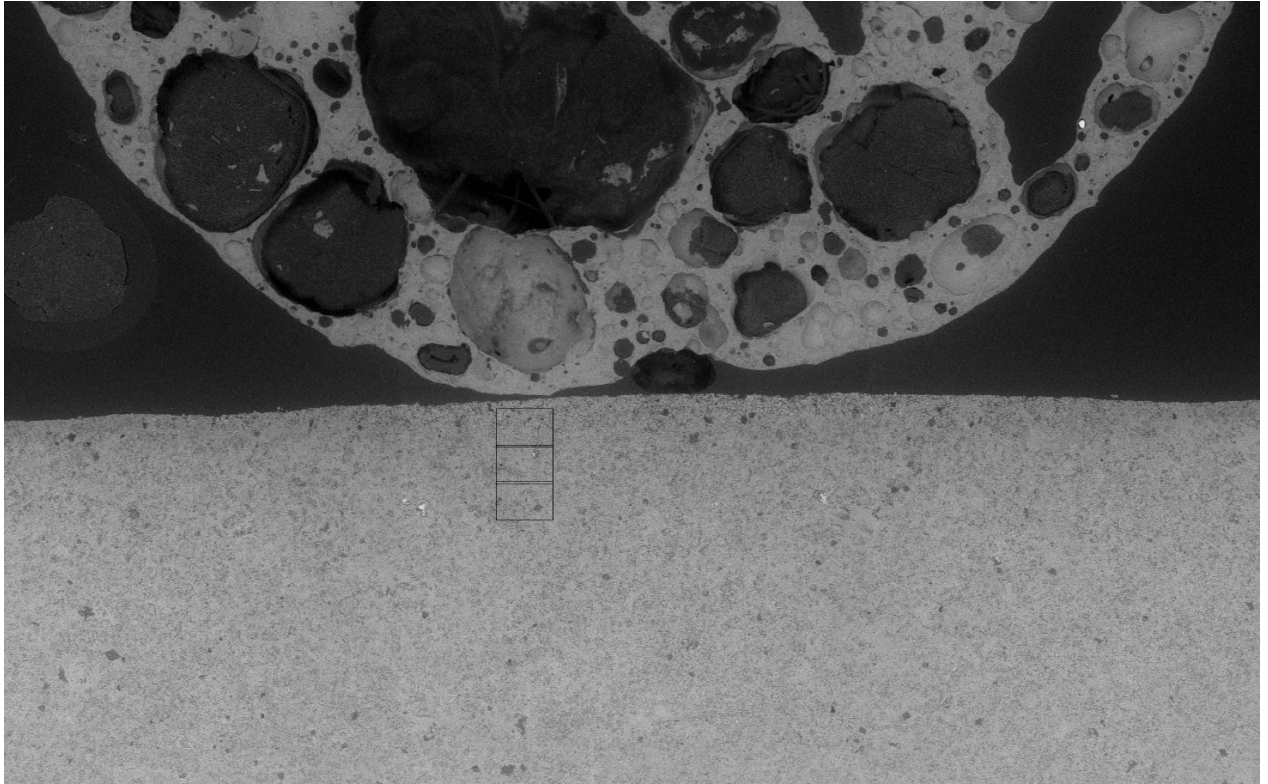


Figure B4 Polished epoxy sample



*Figure B5 Overview of the taken images to analyse the ash infiltration*

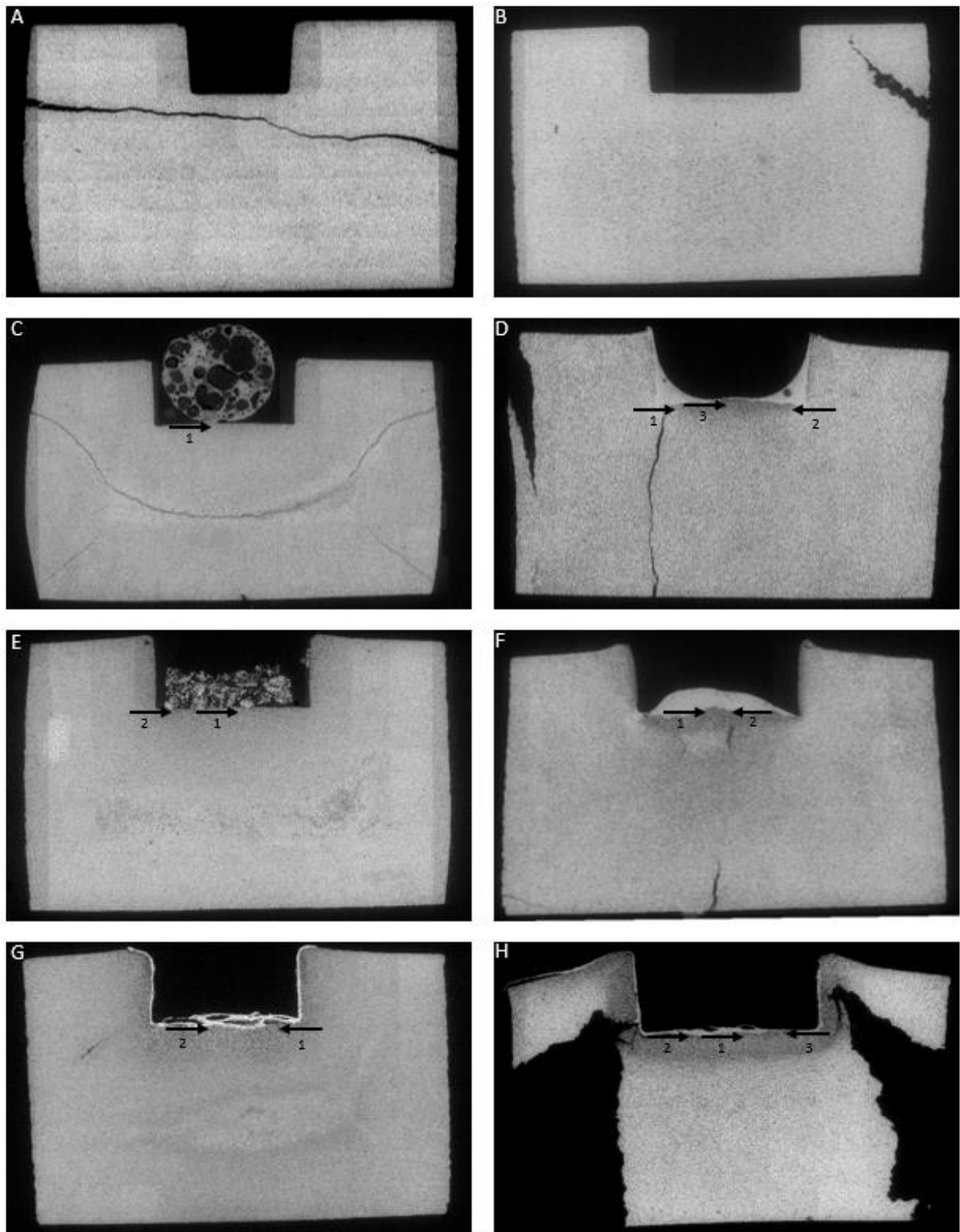


Figure B6 Analysed areas of each sample during the analysing of the ash infiltration, A: Reference 1100°C, B: Reference 1350°C, C: Wheat straw 1100°C, D: Wheat straw 1350°C, E: Forest residues 1100°C, F: Forest residues 1350°C, G: DDGS 1100°C, H: DDGS 1350°C

## Appendix C

```
% Import image original
fds2=fileDatastore('PhotoBatch\\2000x','ReadFcn',@importdata);
fullFileNames2=fds2.Files;

% Import image binary
fds=fileDatastore('PhotoBatch\\2000x_B','ReadFcn',@importdata);
fullFileNames=fds.Files;
numFiles=length(fullFileNames);

for k = 1 : numFiles
    fprintf('Now reading file %s\n', fullFileNames{k}); %binary picture
    Img=read(fds);

%% Display image
close all
h = figure;
set(h,'DefaultFigureWindowStyle','docked');
colormap('gray') % Select a black and white colormap.
subplot(2,3,3)
image(Img) % Display image
axis image % Lock aspect ratio.

%% Generate the lines
NoOfLines = 500;

[Ly,Lx] = size(Img);
LineLength = 700;

Profile=zeros(LineLength,NoOfLines); % making space for the data

hold on
for i =1:NoOfLines
    % generate random position within padded image
    startx = Lx*rand(1);
    starty = Ly*rand(1);
    % generate vector of length L in random direction
    alpha = 2*pi*rand(1);
    dx = LineLength*cos(alpha);
    dy = LineLength*sin(alpha);
    stopx = startx+dx;
    stopy = starty+dy;
    % Following for if-statements makes sure that the whole line fit within
    % the image...
    if stopx < 0 % left side
        startx = startx-stopx;
        stopx = 0;
    end
    if stopx>Lx % right side
        startx = startx-(stopx-Lx);
        stopx = Lx;
    end
    if stopy < 0 % bottom
        starty = starty-stopy;
        stopy = 0;
    end
    if stopy>Ly % top
        starty = starty-(stopy-Ly);
        stopy = Ly;
    end
end
```

```

end
% display line
line([startx stopx],[starty stopy], 'Color', 'r')
% extract image data along lines;
Profile(:,i)= improfile(Img,[startx stopx],[starty stopy],LineLength);
end

%% Proces data
% make binary
Binary=Profile;
Binary(Binary<255)=1; % 1=black=background
Binary(Binary==255)=0; % 0=white=grain

nan=isnan(Binary); %clean
Binary(nan)=[0];

% Porosity: Percentage background (=black=1)
X=sum(Binary);
Porosity=X/LineLength*100;

numWhite=nnz(Img);
numBlack=nnz(~Img);
TotalPorosity=numBlack*100/(numWhite+numBlack); %total porosity picture

% Counting Peaks(Pores)
Peakss=diff(Binary)==1;
Peak=sum(Peakss);

% Length of Pores
PeakStartStop=diff(Binary>0); % Creating a matrix where 1 is equal to the
                                %start point of the pore and -1 is equal to
                                % the end point of the pore

for j=1:NoOfLines % Remove half grains at the beginning and end of the
                  %line
if Binary(1,j)==1;
    Outliers1(1,j)=find(PeakStartStop(:,j)==-1,1, 'first');
    PeakStartStop(Outliers1(:,j),j)=0;
else Outliers1(1,j)=[0];
end

if Binary(LineLength,j)==1;
    Outliers2(1,j)=find(PeakStartStop(:,j)==1,1, 'last');
    PeakStartStop(Outliers2(:,j),j)=0;
else Outliers2(1,j)=[0];
end
end

PeakStart=find(PeakStartStop==1); % x-value of the start point of a pore
PeakStop=find(PeakStartStop==-1); % x-value of the end point of a pore

PoreSize=(PeakStop-PeakStart)*0.144; % Length of the pores and changing
                                     % from pixels to um
m=length(PoreSize)*0.75; %Calculating 3th percentile
n=round(m);
Sort=sort(PoreSize, 'ascend');
P75=Sort(n,1);

```

```

%% Results
Results=zeros(3,4);
Results(1,1)=mean(Peak);
Results(2,1)=std(Peak);
Results(1,2)=P75;
Results(2,2)=mode(PoreSize);
Results(3,2)=median(PoreSize);
Results(1,3)=mean(Porosity);
Results(2,3)=std(Porosity);
Results(1,4)=TotalPorosity;

Results2=array2table(Results,'VariableNames',{'Number_Pores_Mean_std'
        'Pore_Size_P75_Mode_Median' 'Porosity_Mean_std' 'Total_Porosity'});

%% Histograms

subplot(2,3,4)
histogram(Peak,'BinLimits',[10,80],'normalization','probability',
'FaceColor','#4DBEEE','EdgeColor','#4DBEEE');

xlabel('Number of pores')
ylabel('Relative frequency')

subplot(2,3,5)
histogram(Porosity,'BinLimits',[10,90],'normalization','probability',
'FaceColor','#7E2F8E','EdgeColor','#7E2F8E');

xlabel('Porosity (%)')
ylabel('Relative frequency')

subplot(2,3,6)
histogram(PoreSize,'normalization','probability',
'FaceColor','#77AC30','EdgeColor','#77AC30');

xlabel('Pore size (µm)')
ylabel('Relative frequency')

set(h,'DefaultFigureWindowState','docked'); % Original binary picture
subplot(2,3,2)
image(Img);
colormap('gray')
axis image

Img2=read(fds2); % Original picture
subplot(2,3,1)
image(Img2.cdata)
colormap(Img2.colormap);
axis image

%Save
path='x';
saveas(gcf, sprintf([path, '%d.fig'],k)) %save picture

writetable(Results2, sprintf([path, '%d.xls'],k)); %save results

end

```

## Appendix D

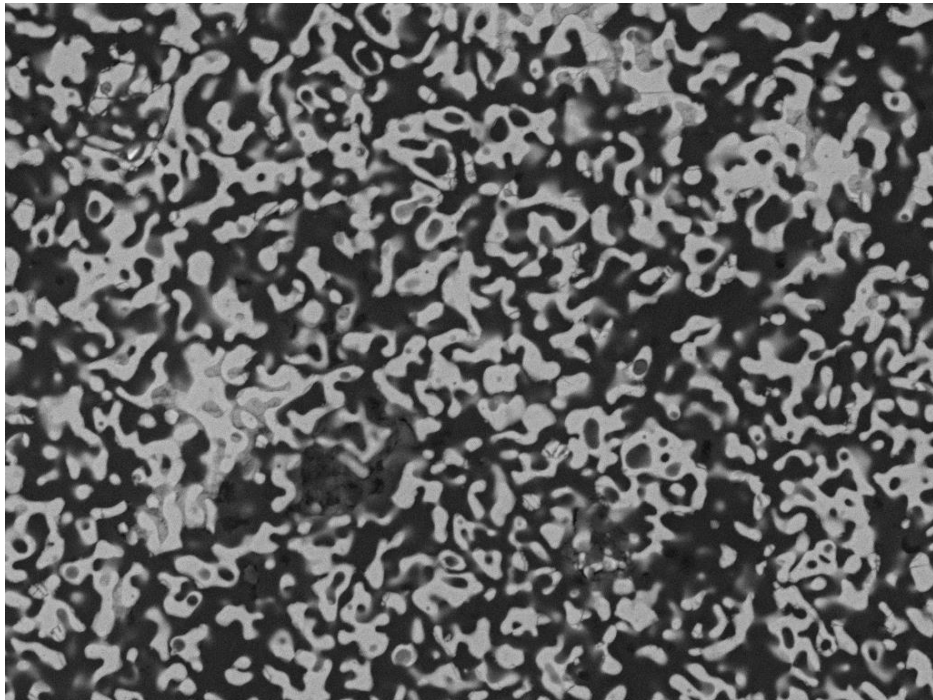


*Figure D7 Original structure image forest residues 1350°C*

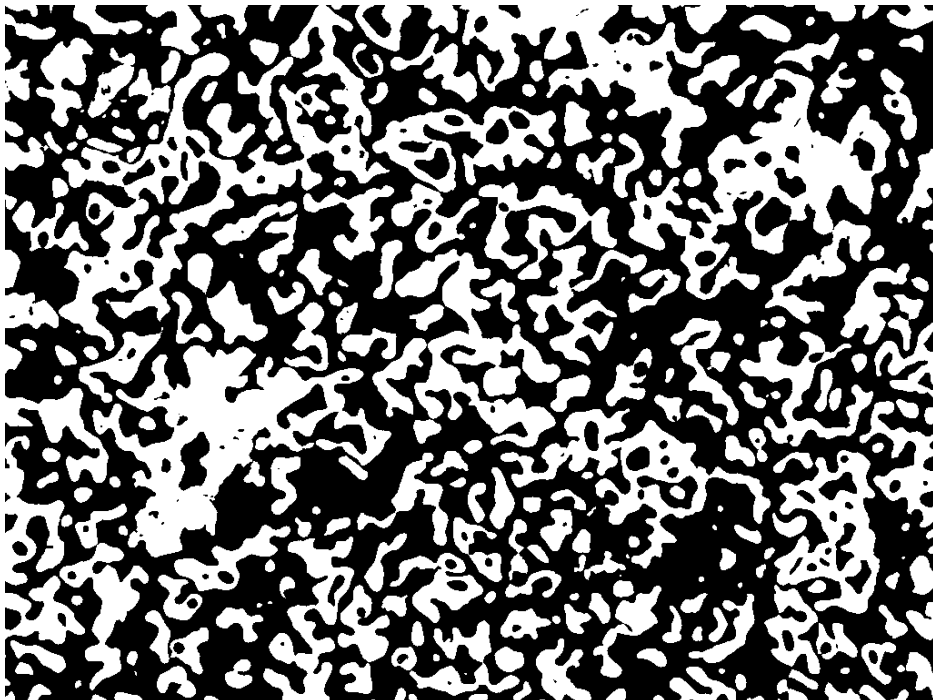


*Figure D8 Image edited with the functions 'smooth' and 'binary', forest residues 1350°C*

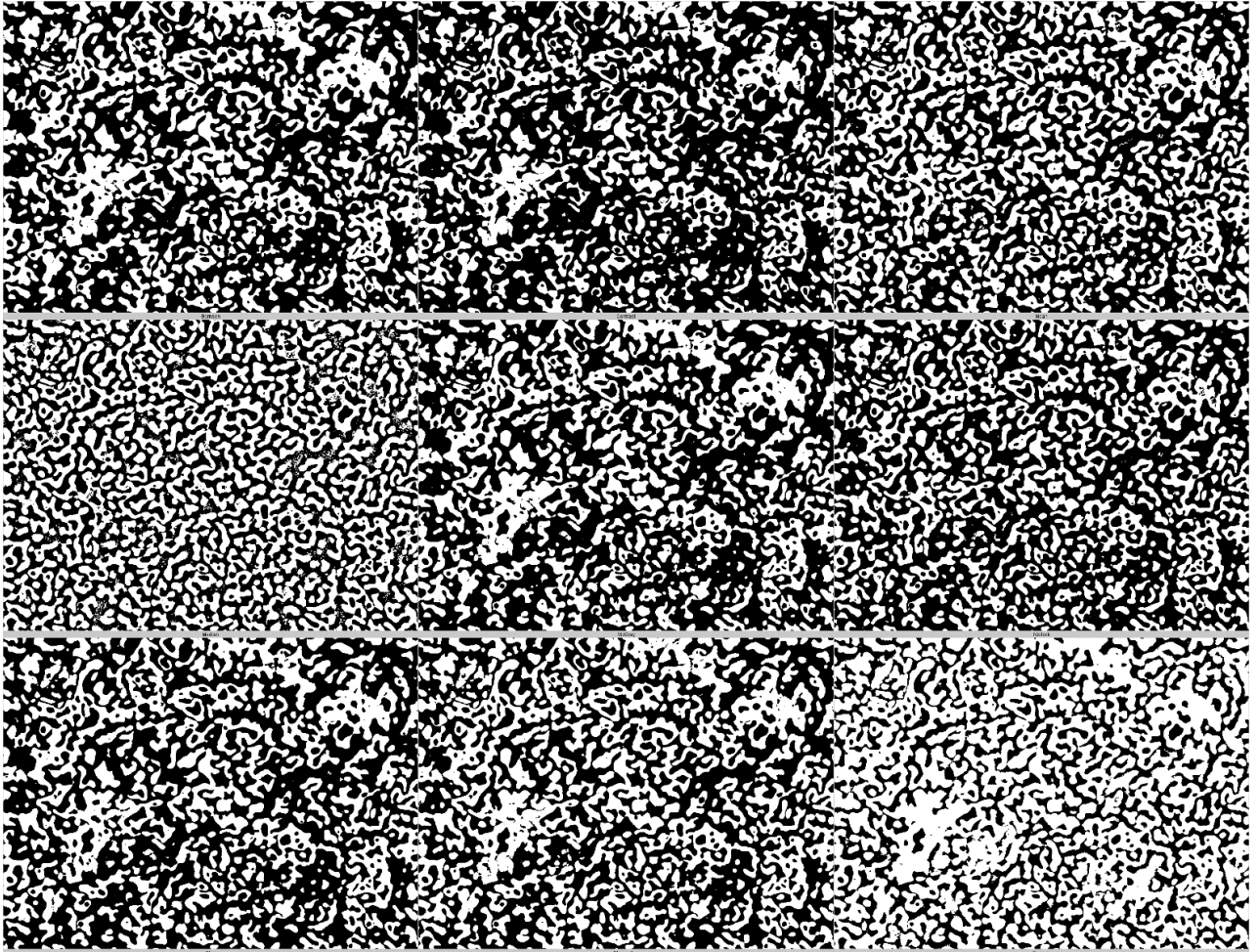


*Figure D9 Image with 'smooth' and 'auto local threshold; R20', forest residues 1350°C*

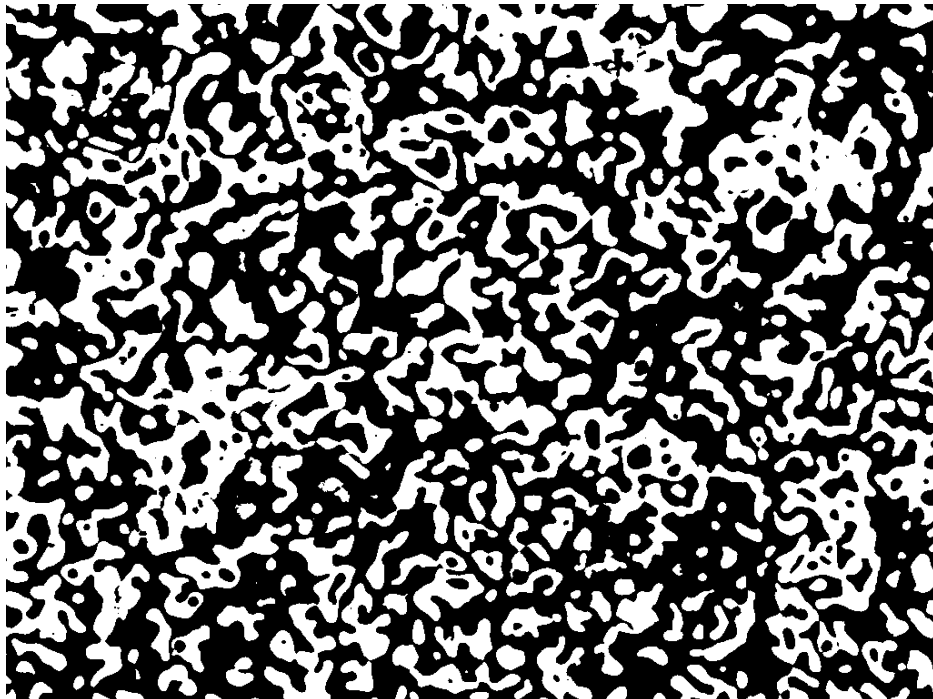


*Figure D10 Image edited with the functions 'smooth' and 'Auto local threshold; Otsu; R20', forest residues 1350°C*

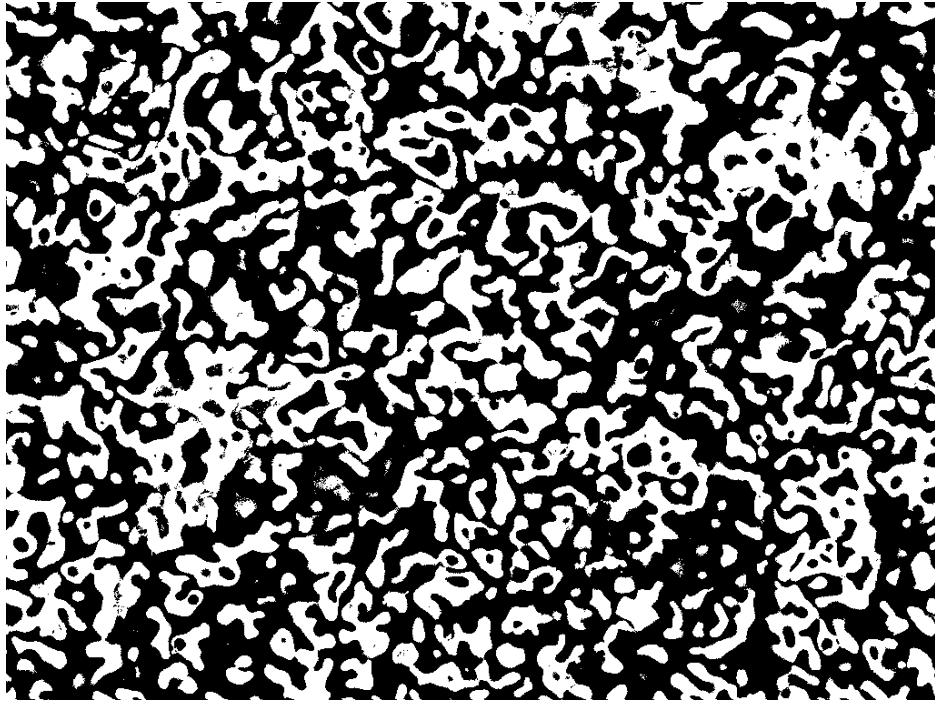


*Figure D11 Image edited with the function 'Auto local threshold; Otsu;R20', forest residues 1350°C*



*Figure D12 Image edited with the functions 'smooth' and 'Auto local threshold; Otsu; R15', forest residues 1350°C*

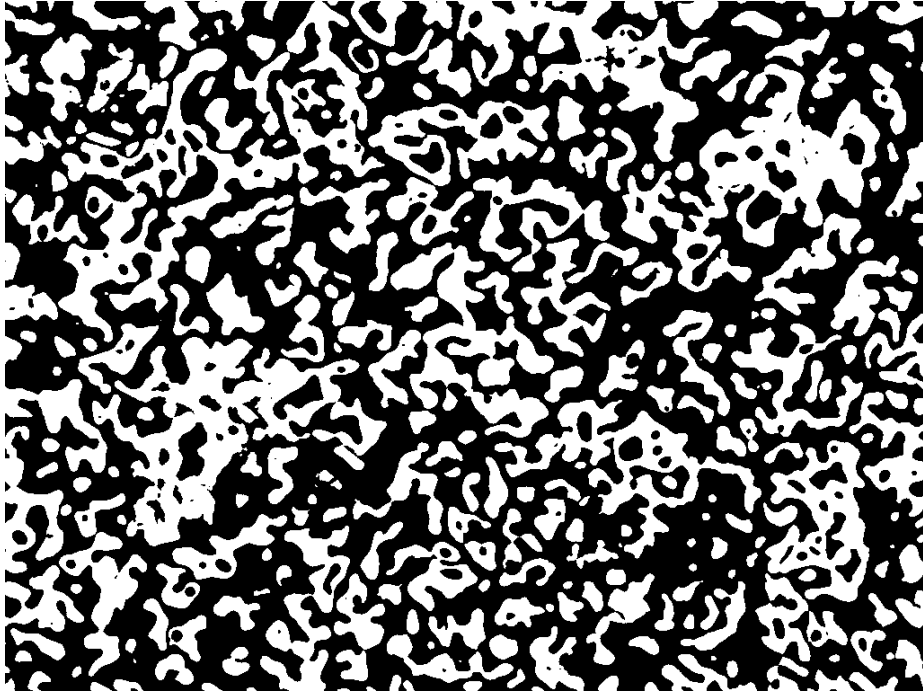


*Figure D13 Image edited with the functions 'smooth' and 'Auto local threshold; Otsu;R25', forest residues 1350°C*

## Appendix E

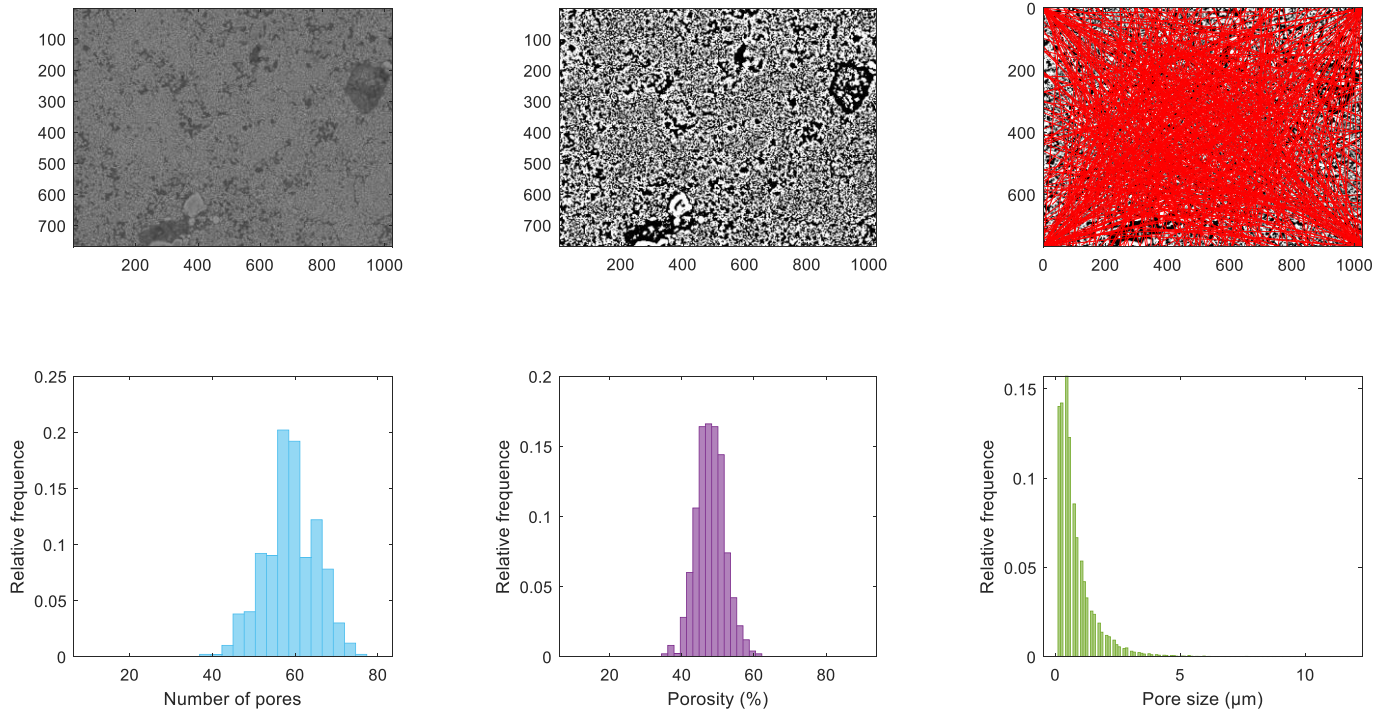


Figure E14 Results of the reference 1100°C sample

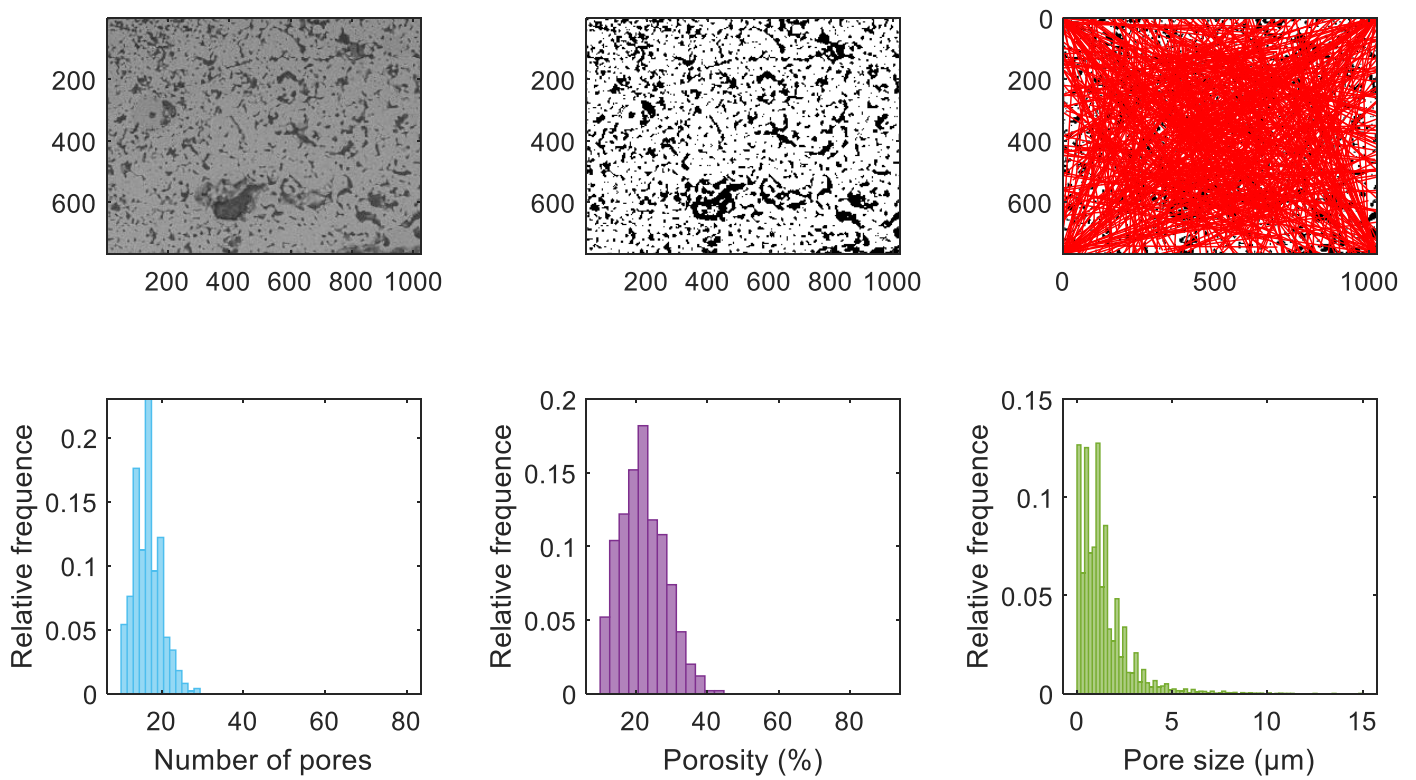


Figure E15 Results of the reference 1350°C sample

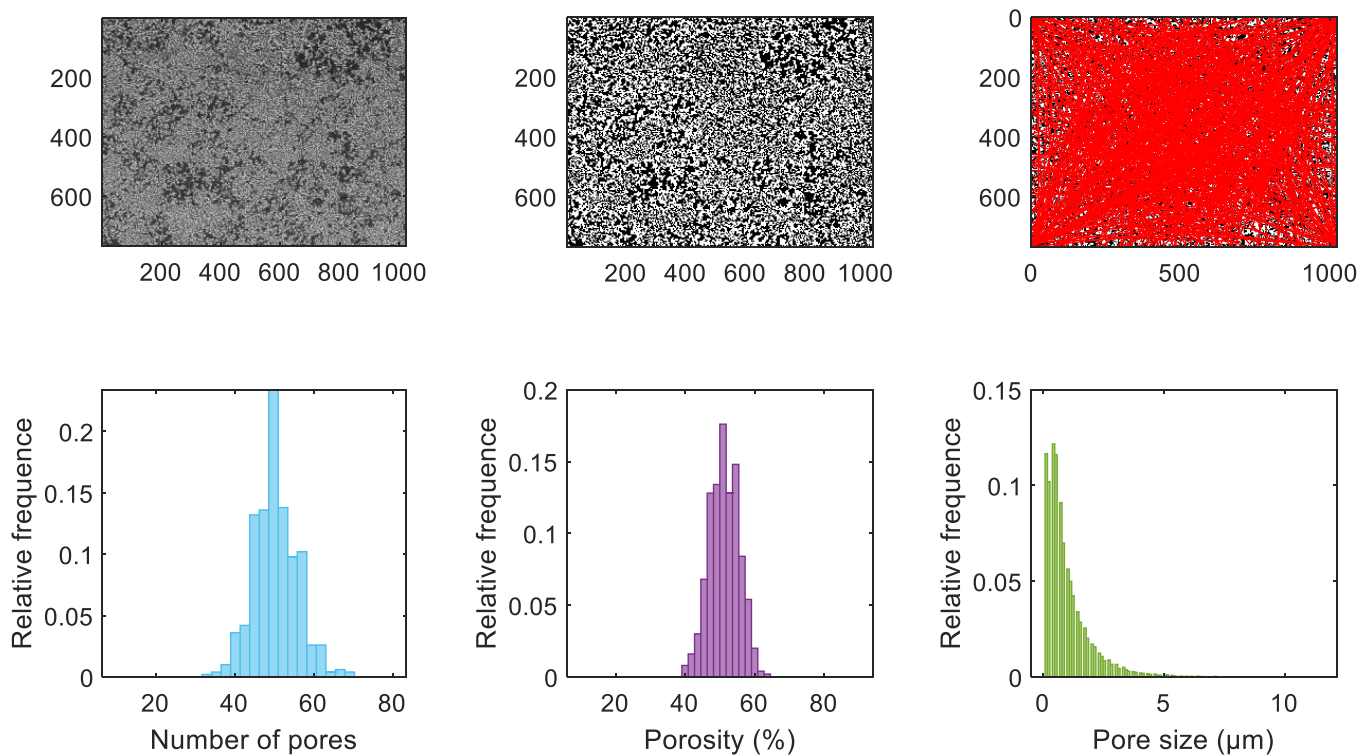


Figure E16 Results of the wheat straw 1100°C sample

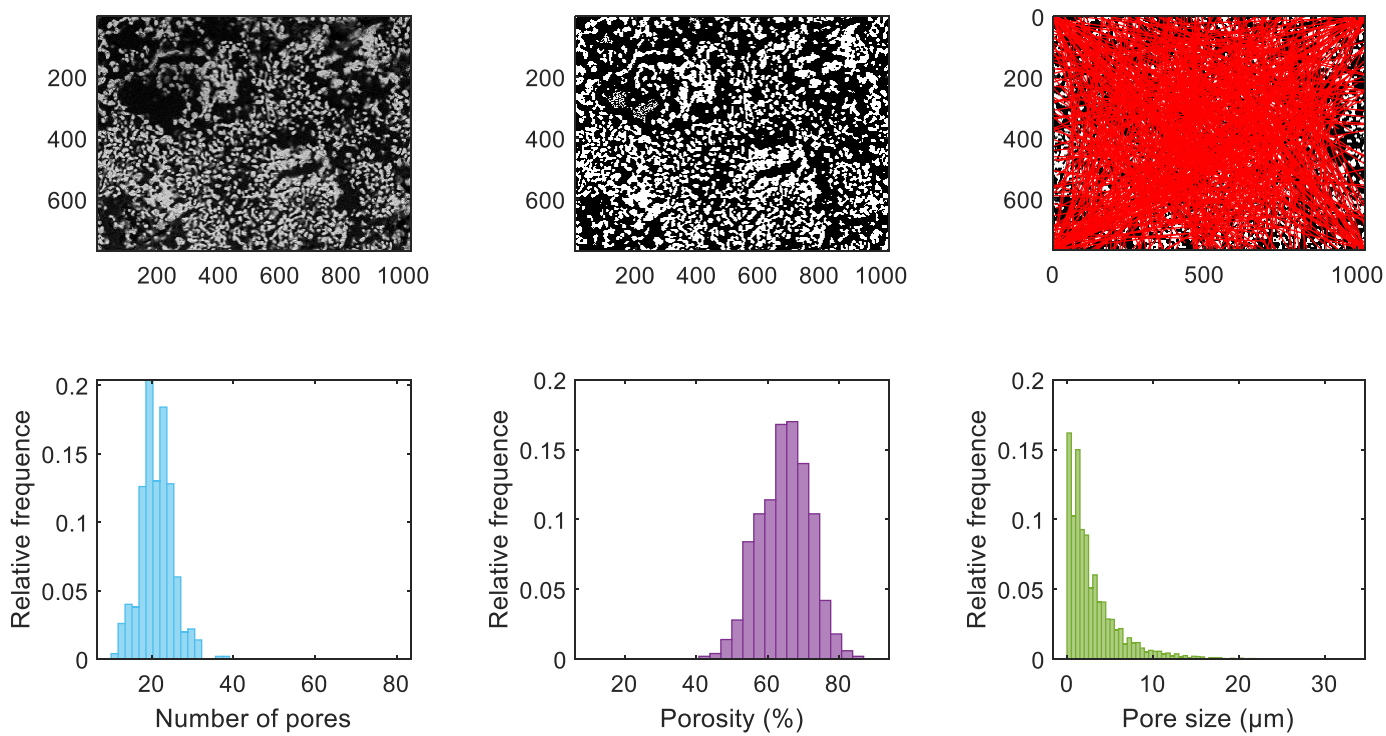


Figure E17 Results of the wheat straw 1350°C sample

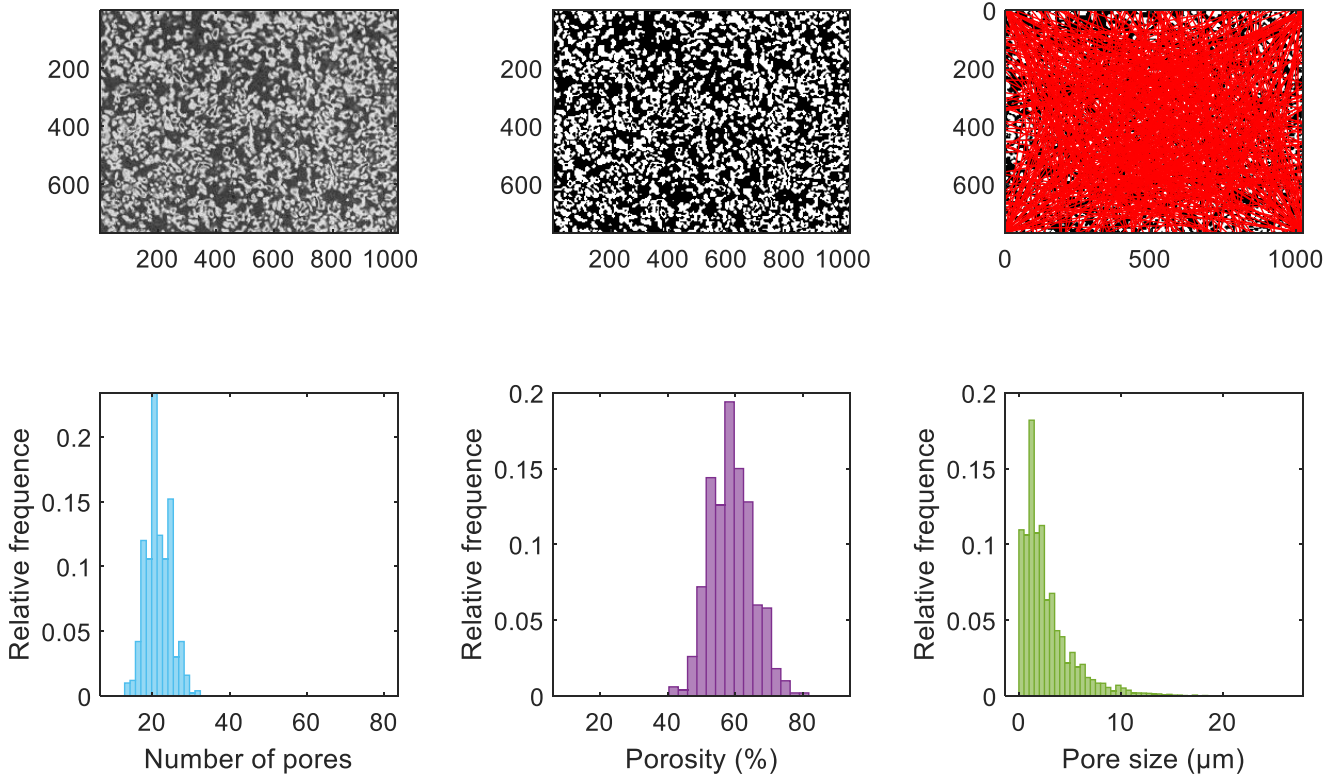


Figure E18 Results of the forest residue 1100°C sample

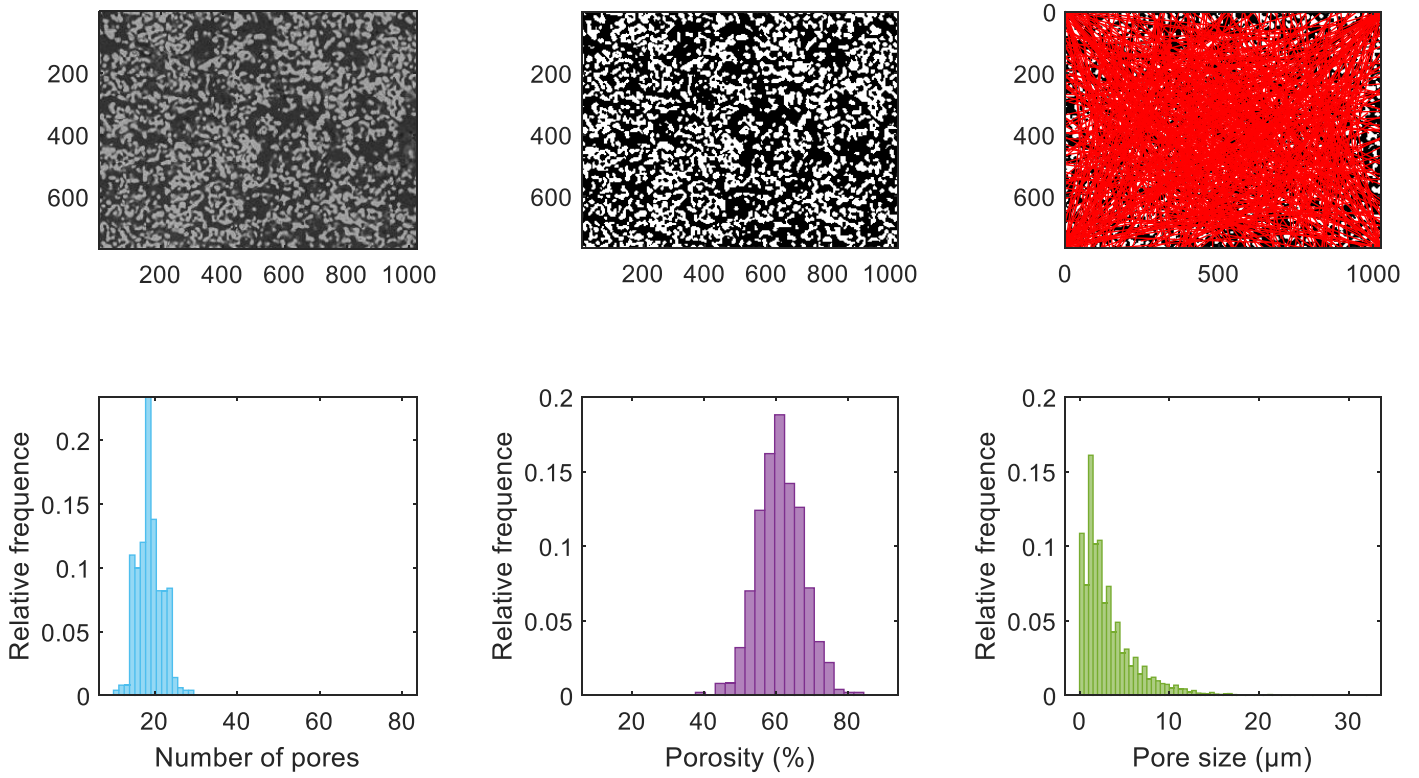


Figure E19 Results of the forest residue 1350°C sample

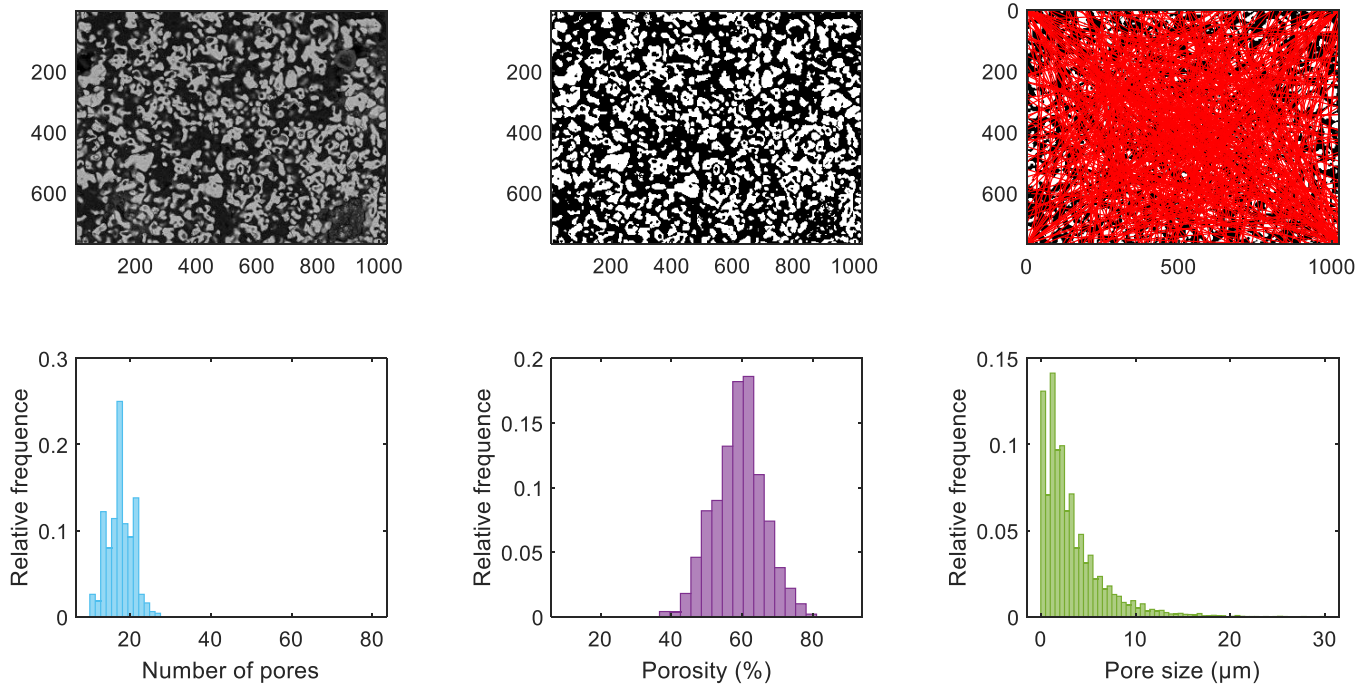


Figure E20 Results of the DDGS 1100°C sample

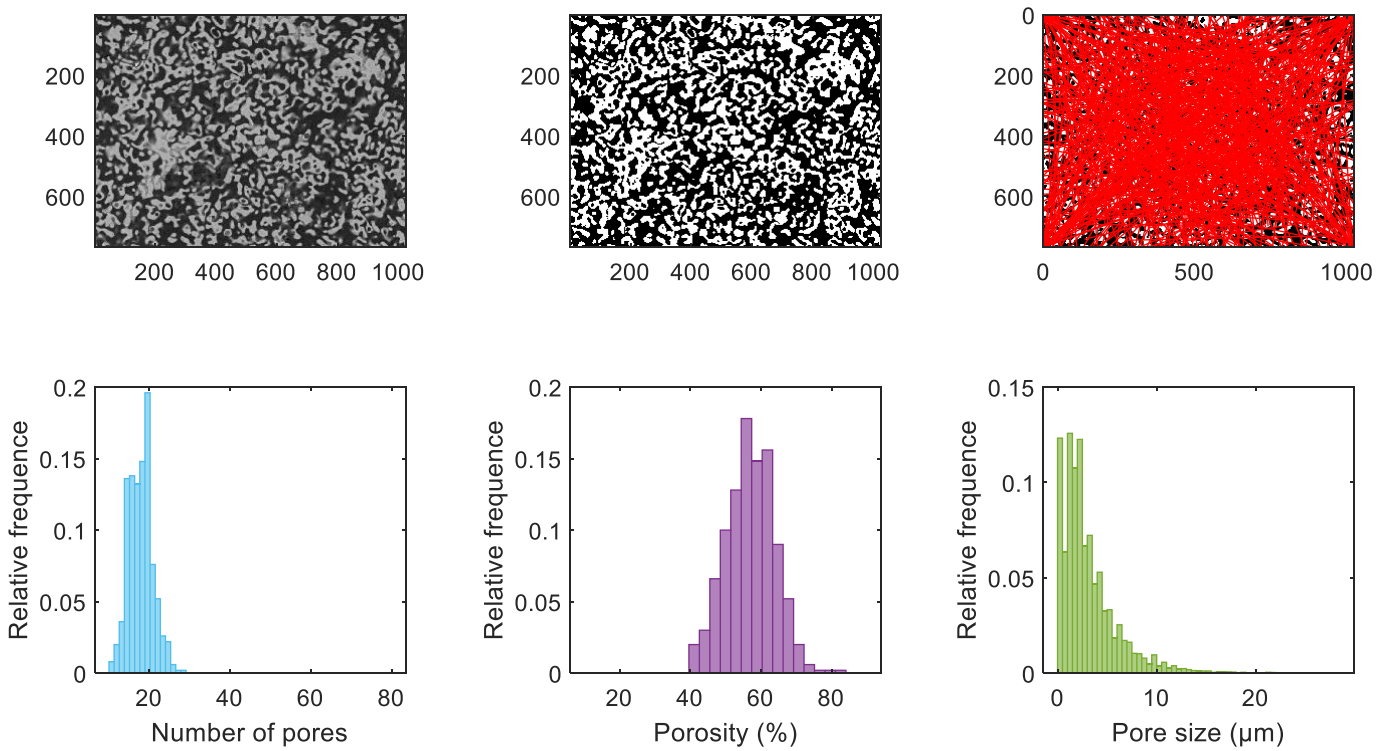


Figure E21 Results of the DDGS 1350°C sample